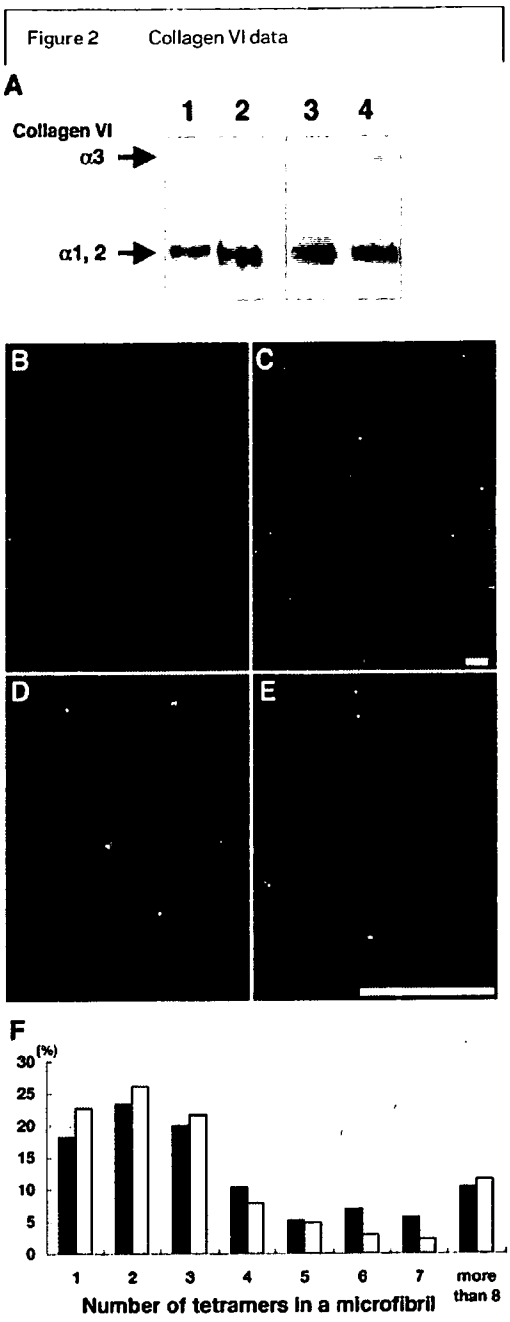

(A) Collagen VI in the fibroblasts or the cultured medium. Collagen VI is present in the extract of cells on dish (lane 1, control cells; lane 2, p.G284R mutation) and in the cultured medium of cells (lane 3, control cells; lane 4, p.G284R mutation). Collagen VI with p.G284R is produced and secreted to cultured medium in the same mass and amount compared to control cells. (B through E) Negative staining electron microscopy of secreted collagen VI. Collagen VI microfibrils in the cultured medium secreted from control cells (B, D) or cells with this p.G284R mutation (C, E) were visualized by negative staining electron microscopy. Long microfibrils are present in both control and patient (B, C). The magnified images show that the structure of tetramer is normal in length and shape. Bars denote 100 nm (D, E). (F) Quantitative analysis of association of collagen VI tetramers. The distribution of the numbers of tetramer in one microfibril is shown as a percentage of the total number of microfibrils. Black bars show the results of 231 microfibrils from control cells. White bars show 163 microfibrils from Ullrich congenital muscular dystrophy patient cells.

of collagen VI deficient cells retained on dish (bar no. 6 in figure 4A). Our analysis of substrate-retained collagen VI supported these findings. Only after treatment with the cultured medium containing normal collagen VI, we observed the recovery of substrate-retained collagen VI in the patient's cells with p.G284R mutation and collagen VI deficiency (figure 4B, lanes 3, 5). However, the addition of the cultured medium containing collagen VI with p.G284R mutation did not recover the reduction of the amount of collagen VI in the ECM of p.G284R mutated and collagen VI deficient cells (figure 4B, lanes 4, 6). In contrast, the amount of fibronectin bound to the substrate showed no difference between control and the mutant cells (figure 4B).

We further analyzed the remaining proteins bound to the substrate in order to examine influences of the alteration of collagen VI molecule to other proteins. In the 2D-PAGE analysis, only two groups of spots from 937 spots detected showed marked reduction (>fivefold) in the patient with p.G284R as compared to control. MALDI-TOF-mass spectrometry analysis revealed that these proteins were collagen VI α 1 and α 2. In contrast, the amount of the other substrate-bound proteins on dish was not greatly altered (see supplemental data at www.neurology.org).

DISCUSSION In this study, we used fibroblasts from patients with UCMD with heterozygous c.850G>A (p.G284R) mutation in *COL6A1* gene in the *N*-terminal region of the triple helical domain. Mutations in this region have been reported to be associated with UCMD and Bethlem myopathy.[12-16] Muscles from all four patients with this mutation showed the characteristic features of SSCD, just as in previously reported patients.[2,12,14,22] In our series, we were not able to establish genotype-phenotype correlation between SSCD and complete deficiency of collagen VI.

On electron microscopy, the shape and the length of collagen VI microfibrils secreted from cultured fibroblasts from the patients seemed to be normal, indicating that the mutation of p.G284R does not affect the production and formation of the microfibrils. Our data contradict previous reports showing that mutations in the triple helical domain of *COL6A1* are associated with abnormal tetramer formation and unnaturally long microfibrils.[12,17] These results suggest that glycine substitution in the triple helical do-

Figure 3 Immunocytochemical staining of collagen VI binding to the cells with the complete deficiency of collagen VI

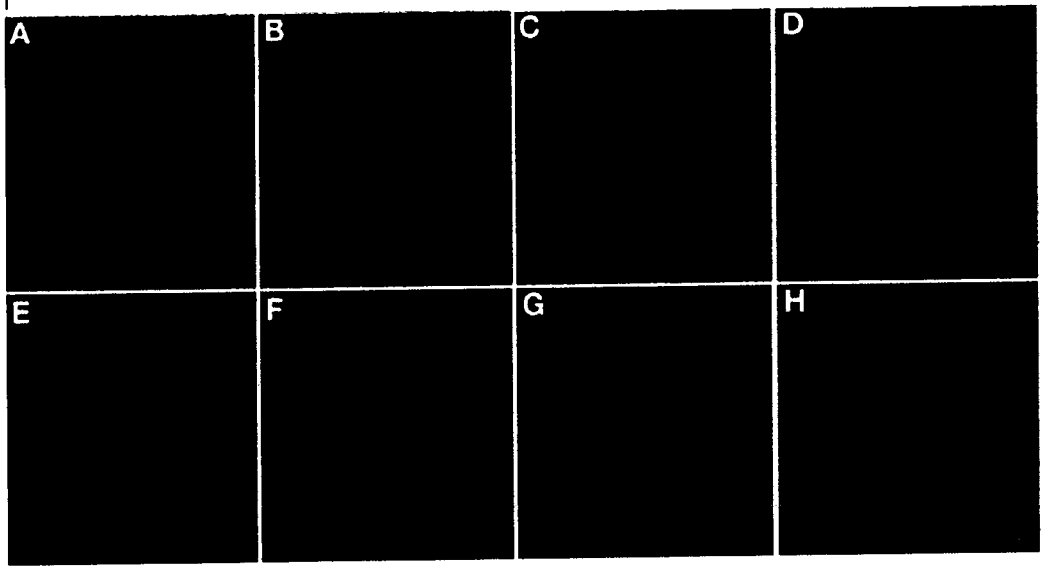

Collagen VI (green) is clearly present in extracellular area of the control fibroblasts (A). In the cells of complete deficiency, collagen VI is absent (E). Culturing with control medium (B, 1 day; C, 2 days; D, 3 days) or in p.G284R medium (F, 1 day; G, 2 days; H, 3 days). In culture with control medium, collagen VI is present on dish on days 2 and 3; in p.G248R medium (F through H), collagen VI is detected on dish on day 3 in extremely reduced amount. Bar denotes 20 μm. Nuclei of cells are stained with TOTO-3 (blue)

main may cause a variety of influences on the formation of collagen VI.

We evaluated the function of mutated collagen VI in p.G284R using patients with UCMD's fibroblasts. The immunocytochemical staining of the collagen VI deficient cells after incubation with cultured medium clearly show that collagen VI in the cultured medium of UCMD cells with p.G284R mutation had less binding capacity than that of control cells. These results suggest that the microfibrils with the mutated collagen VI α1 chain alter the affinity of collagen VI to its binding partners. Previous studies showed the presence of aggregated filaments sometimes assuming dot/spot-like appearance in the fibroblasts with the same mutation p.G284R,[14] which may support our contention that the alteration in the collagen VI microfibrils by this mutation can influence the interaction of collagen VI microfibrils in ECM.

The results in the cell attachment test demonstrated that the adhesion ability of cells with the p.G284R and complete deficiency of collagen VI was less compared to that of control cells. The amount of the retained collagen VI on dish after the washing was reduced in the patients with UCMD (p.G284R and collagen VI complete deficiency) compared to control. These findings suggested that the reduction of the binding capacity by p.G284R mutation may cause an abnormality in the adhesion of fibroblasts from patients with UCMD. Since collagen VI is thought to anchor cells to the ECM, loss of the binding capacity should result in reduced cell adhesion. Our findings indicate that the interaction of collagen VI is related to cell adhesion between fibroblasts and ECM.

The specific loss of collagen VI in sarcolemma of these patients, which is the pathologic finding in muscle sections, suggests a possibility that this feature may be caused by the reduction of binding capacity of collagen VI microfibrils to other molecules as a results of the heterozygous mutation in the *COL6A1* triple helical domain. Collagen VI microfibrils have been shown to bind to cell-surface receptors, integrins,[23] and NG2,[24,25] and interact with several ECM components including fibrillar collagens,[26,27] collagen IV,[28] fibronectin,[29,30] biglycan, decorin,[31-33] and microfibril-associated glycoprotein-1 (MAGP-1).[34] Further studies on the binding partners of collagen VI in the ECM or on the cellular membrane may provide clues in understanding the function of collagen VI and the pathomechanism behind UCMD.

Our results on the mutant cells cultured in normal medium are of note. Interestingly, the adhesion ability of the cells with *COL6A1* p.G284R mutation and complete deficiency was restored by switching the medium to the one containing normal collagen VI microfibrils, indicating that

Figure 4 Recovery of binding ability of patients with Ullrich congenital muscular dystrophy (UCMD)'s cells by changing cultured medium from normal or p.G284R fibroblasts

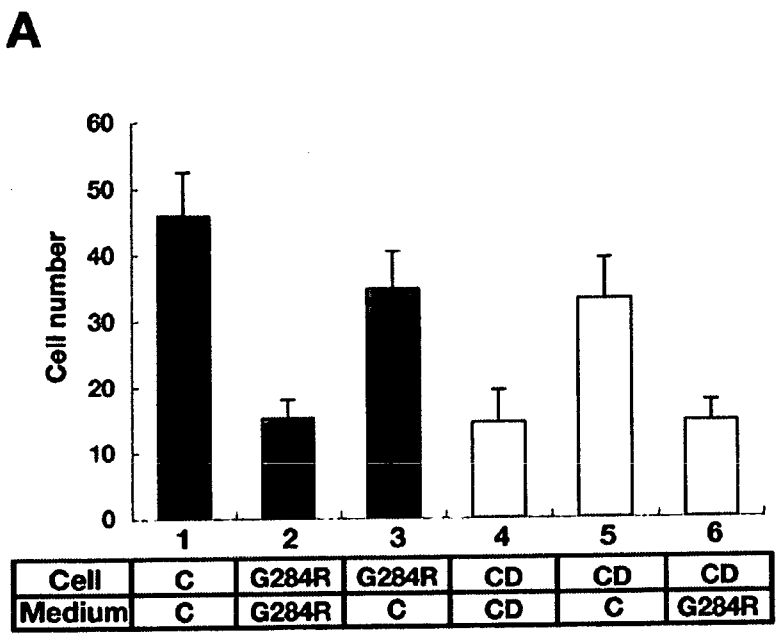

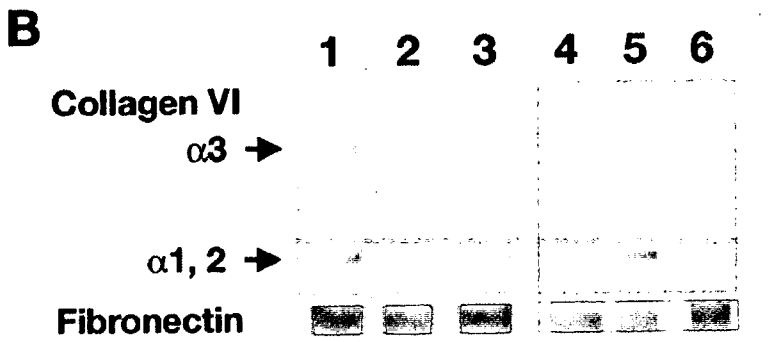

(A) Number of remaining cells on the dish after detachment with EDTA solution. After changing into control medium (containing collagen VI), the number of cells became comparable to control (no 1). On the other hand, UCMD cells, p.G284R (gray bar, no. 2), or collagen VI complete deficiency (open bar, no 4), whose medium have not been changed, do not show recovery of cell attachment ($p < 0.001$, the number of counted area = 8). The cultured medium containing collagen VI with p G284R likewise can not restore adhesion capacity of collagen VI complete deficiency cells (open bar, no 6). Error bars indicate standard deviations. (B) The cells are cultured in three types of medium: original medium from cells (lanes 1, 2, 4); medium from control cells containing normal collagen VI (lanes 3, 5); or medium from cells with p G284R mutation (lane 6). After the detachment of the cells by 10 mM EDTA, collagen VI is observed in control cells (lane 1). Cells with p.G284R mutation cultured in their own medium showed no detectable collagen VI (lane 2); however, after culture in the normal medium, collagen VI is observed in similar amounts to the control cells (lane 3). In collagen VI deficient cells, collagen VI is deficient in their own medium, but is detected when normal medium is used (lane 5). Interestingly, medium from p G284R cells contains similar amounts of collagen VI protein to control cells (figure 2, lane 4), but collagen VI deficient cells cultured in this medium showed no detectable collagen VI (lane 6).

the function of mutant fibroblasts can be rescued by adding normal collagen VI. Moreover, recovering only by the addition of cultured medium containing normal collagen VI indicates that other functions and molecules of cells from patients with UCMD are normal. Results of recovery test using collagen VI-deficient fibroblasts suggested that collagen VI microfibrils with p.G284R mutation are less likely to interact with collagen VI binding partners, and thus, affecting the function of cells in attaching to other ECM proteins. These results demonstrated that the addition of normal collagen VI microfibrils possessing intact affinity to its binding partners rescues abnormalities in these cells from UCMD. This denotes that therapeutic use of normal collagen VI in patients with UCMD with SSCD may be plausible.

ACKNOWLEDGMENT

The authors thank the patients and their families for their cooperation and support of this research; K. Murayama and F. Uematsu for technical assistance; and May Christine V. Malicdan, MD (NCNP), for English revision of the manuscript.

Received December 28, 2006. Accepted in final form April 9, 2007.

REFERENCES

1. Ullrich O. Kongenitale, atonisch-sklerotische Muskeldystrophie, ein weiterer Typus der heredodegenerativen Erkrankungen des neuromuskulären Systems. Z Ges Neurol Psychiatry 1930;126:171–201.
2. Ishikawa H, Sugie K, Murayama K, et al. Ullrich disease due to deficiency of collagen VI in the sarcolemma. Neurology 2004;62:620–623.
3. Camacho Vanegas O, Bertini E, Zhang RZ, et al. Ullrich scleroatonic muscular dystrophy is caused by recessive mutations in collagen type VI. Proc Natl Acad Sci USA 2001;98:7516–7521.
4. Mercuri E, Yuva Y, Brown SC, et al. Collagen VI involvement in Ullrich syndrome: a clinical, genetic, and immunohistochemical study. Neurology 2002;58:1354–1359.
5. Ishikawa H, Sugie K, Murayama K, et al. Ullrich disease: collagen VI deficiency: EM suggests a new basis for muscular weakness. Neurology 2002;59:920–923.
6. Higuchi I, Shiraishi T, Hashiguchi T, et al. Frameshift mutation in the collagen VI gene causes Ullrich's disease. Ann Neurol 2001;50:261–265.
7. Weil D, Mattei MG, Passage E, N'Guyen VC, et al. Cloning and chromosomal localization of human genes encoding the three chains of type VI collagen. Am J Hum Genet 1998;42:435–445.
8. Ball S, Bella J, Kielty C, Shuttleworth A. Structural basis of type VI collagen dimer formation. J Biol Chem 2003;278:15326–15332.
9. Baldock C, Sherratt MJ, Shuttleworth CA, Kielty CM. The supramolecular organization of collagen VI microfibrils. J Mol Biol 2003;330:297–307.
10. Sherratt MJ, Holmes DF, Shuttleworth CA, Kielty CM. Substrate-dependent morphology of supramolecular assemblies: fibrillin and type-VI collagen microfibrils. Biophys J 2004;86:3211–3222.
11. Lamandé SR, Sigalas E, Pan TC, et al. The role of the alpha 3 (VI) chain in collagen VI assembly. Expression of an alpha 3 (VI) chain lacking N-terminal modules

N10-N7 restores collagen VI assembly, secretion, and matrix deposition in an alpha 3 (VI)-deficient cell line. J Biol Chem 1998;273:7423–7430.
12. Baker NL, Mörgelin M, Peat R, et al. Dominant collagen VI mutations are a common cause of Ullrich congenital muscular dystrophy. Hum Mol Genet 2005;14:279–293.
13. Lampe AK, Dunn DM, von Niederhausern C, et al. Automated genomic sequence analysis of the three collagen VI genes: applications to Ullrich congenital muscular dystrophy and Bethlem myopathy. J Med Genet 2005;42:108–120.
14. Giusti B, Lucarini L, Pietroni V, et al. Dominant and recessive COL6A1 mutations in Ullrich scleroatonic muscular dystrophy. Ann Neurol 2005;58:400–410.
15. Lampe AK, Bushby KM. Collagen VI related muscle disorders. J Med Genet 2005;42:673–685.
16. Lucioli S, Giusti B, Mercuri E, et al. Detection of common and private mutations in the COL6A1 gene of patients with Bethlem myopathy. Neurology 2005;64:1931–1937.
17. Lamandé SR, Mörgelin M, Selan C, Jobsis GJ, Baas F, Bateman JF. Kinked collagen VI tetramers and reduced microfibril formation as a result of Bethlem myopathy and introduced triple helical glycine mutations. J Biol Chem 2002;277:1949–1956.
18. Bethlem J, Wijngaarden GK. Benign myopathy, with autosomal dominant inheritance. A report on three pedigrees. Brain 1976;99:91–100.
19. Jobsis GJ, Keizers H, Vreijling JP, et al. Type VI collagen mutations in Bethlem myopathy, an autosomal dominant myopathy with contractures. Nat Genet 1996;14:113–115.
20. Pan TC, Zhang RZ, Pericak-Vance MA, et al. Missense mutation in a von Willebrand factor type A domain of the alpha 3(VI) collagen gene (COL6A3) in a family with Bethlem myopathy. Hum Mol Genet 1998;7:807–812.
21. Pepe G, Giusti B, Bertini E, et al. A heterozygous splice site mutation in COL6A1 leading to an in-frame deletion of the alpha 1(VI) collagen chain in an Italian family affected by Bethlem myopathy. Biochem Biophys Res Commun 1999;258:802–807.
22. Pan TC, Zhang RZ, Sudano DG, Marie SK, Bonnemann CG, Chu ML. New molecular mechanism for Ullrich congenital muscular dystrophy: a heterozygous in-frame deletion in the COL6A1 gene causes a severe phenotype. Am J Hum Genet 2003;73:355–369.
23. Tulla M, Pentikainen OT, Viitasalo T, et al. Selective binding of collagen subtypes by integrin alpha 1I, alpha 2I, and alpha 10I domains. J Biol Chem 2001;276:48206–48212.
24. Burg MA, Tillet E, Timpl R, Stallcup WB. Binding of the NG2 proteoglycan to type VI collagen and other extracellular matrix molecules. J Biol Chem 1996;271:26110–26116.
25. Tillet E, Ruggiero F, Nishiyama A, Stallcup WB. The membrane-spanning proteoglycan NG2 binds to collagens V and VI through the central nonglobular domain of its core protein. J Biol Chem 1997;272:10769–10776.
26. Keene DR, Engvall E, Glanville RW. Ultrastructure of type VI collagen in human skin and cartilage suggests an anchoring function for this filamentous network. J Cell Biol 1988;107:1995–2006.
27. Bonaldo P, Russo V, Bucciotti F, Doliana R, Colombatti A. Structural and functional features of the 3 chain indicate a bridging role for chicken collagen VI in connective tissues. Biochemistry 1990;29:1245–1254.
28. Kuo HJ, Maslen CL, Keene DR, Glanville RW. Type VI collagen anchors endothelial basement membranes by interacting with type IV collagen. J Biol Chem 1997;272:26522–26529.
29. Tillet E, Wiedemann H, Golbik R, et al. Recombinant expression and structural and binding properties of alpha 1 (VI) and alpha 2 (VI) chains of human collagen type VI. Eur J Biochem 1994;221:177–185.
30. Sabatelli P, Bonaldo P, Lattanzi G, et al. Collagen VI deficiency affects the organization of fibronectin in the extracellular matrix of cultured fibroblasts. Matrix Biol 2001;20:475–486.
31. Wiberg C, Klatt AR, Wagener R, et al. Complexes of matrilin-1 and biglycan or decorin connect collagen VI microfibrils to both collagen II and aggrecan. J Biol Chem 2003;278:37698–37704.
32. Wiberg C, Heinegard D, Wenglen C, Timpl R, Mörgelin M. Biglycan organizes collagen VI into hexagonal-like networks resembling tissue structures. J Biol Chem 2002;277:49120–49126.
33. Wiberg C, Hedbom E, Khairullina A, et al. Biglycan and decorin bind close to the n-terminal region of the collagen VI triple helix. J Biol Chem 2001;276:18947–18952.
34. Finnis ML, Gibson MA. Microfibril-associated glycoprotein-1 (MAGP-1) binds to the pepsin-resistant domain of the alpha 3 (VI) chain of type VI collagen. J Biol Chem 1997;272:22817–22823.

Human Molecular Genetics, 2007, Vol. 16, No. 22 2669–2682
doi:10.1093/hmg/ddm220
Advance Access Published on August 18, 2007

A *Gne* knockout mouse expressing human *GNE* D176V mutation develops features similar to distal myopathy with rimmed vacuoles or hereditary inclusion body myopathy

May Christine V. Malicdan, Satoru Noguchi*, Ikuya Nonaka, Yukiko K. Hayashi and Ichizo Nishino

Department of Neuromuscular Research, National Institute of Neuroscience, National Center of Neurology and Psychiatry, 4-1-1 Ogawahigashi-cho, Kodaira, Tokyo 187-8502, Japan

Received July 27, 2007; Revised July 27, 2007; Accepted August 7, 2007

Distal myopathy with rimmed vacuoles (DMRV) or hereditary inclusion body myopathy (hIBM) is an early adult-onset distal myopathy caused by mutations in the UDP-*N*-acetylglucosamine 2-epimerase/*N*-acetylmannosamine kinase (*GNE*) gene which encodes for a bifunctional enzyme involved in sialic acid biosynthesis. It is pathologically characterized by the presence of rimmed vacuoles (RVs), especially in atrophic fibers, which also occasionally contain congophilic materials that are immunoreactive to β-amyloid, lysosomal proteins, ubiquitin and tau proteins. To elucidate the pathomechanism of this myopathy and to explore treatment options, we generated a mouse model of DMRV/hIBM. We knocked out the *Gne* gene in mice but this resulted in embryonic lethality. We therefore generated a transgenic mouse that expressed the human *GNE* D176V mutation, which is one of the most prevalent mutations among Japanese DMRV patients, and crossed this with $Gne^{(+/-)}$ mice to obtain $Gne^{(-/-)}$h*GNE*D176V-Tg. Interestingly, these mice exhibit marked hyposialylation in serum, muscle and other organs. Reduction in motor performance in these mice can only be seen from 30 weeks of age. A compelling finding is the development of β-amyloid deposition in myofibers by 32 weeks, which clearly precedes RV formation at 42 weeks. These results show that the $Gne^{(-/-)}$h*GNE*D176V-Tg mouse mimics the clinical, histopathological and biochemical features of DMRV/hIBM, making it useful for understanding the pathomechanism of this myopathy and for employing different strategies for therapy. Our findings underscore the notion that hyposialylation plays an important role in the pathomechanism of DMRV/hIBM.

INTRODUCTION

Distal myopathy with rimmed vacuoles (DMRV) is an autosomal recessive myopathy that was originally reported by Nonaka *et al.* (1), and thus it is also known as Nonaka myopathy. It is the same entity with hereditary inclusion body myopathy (hIBM), which was initially reported among Iranian Jews (2). DMRV/hIBM usually starts to affect adults from 15 years of age up to 40 years, with an average onset of 26 years and with an initial symptom of altered gait (1). It is gradually progressive, and patients become wheelchair-bound between 26 and 57 years of age, or about an average of 12 years after the onset of symptoms (3).

DMRV/hIBM is characterized by preferential involvement of the distal muscles of lower extremities, especially the tibialis anterior muscles, with relative sparing of the quadriceps, and hence the term 'quadriceps-sparing' rimmed vacuolar myopathy (2). Other muscles are involved as well, especially late in the course of the disease (3). Serum creatine kinase

*To whom correspondence should be addressed. Tel: +81 423461712; Fax: +81 423461742; Email: noguchi@ncnp.go.jp

(CK) level is normal or mildly elevated. The characteristic finding on muscle biopsy is the presence of rimmed vacuoles (RVs), which are actually empty spaces surrounded by aggregation of autophagic vacuoles. These RVs occasionally contain congophilic materials that are immunoreactive to various proteins, including β-amyloid, phosphorylated tau, ubiquitin and α-synuclein. Necrotic and regenerating fibers and areas of inflammation are uncommon but can be seen. Ultrastructurally, filamentous inclusions measuring 18–20 nm in diameter are seen in both the cytoplasm and the nucleus (3), in addition to the presence of autophagy and various inclusions.

DMRV/hIBM was mapped to chromosome 9 (4,5) and was shown to be associated to mutations in the *GNE* gene (6,7), which encodes for a bifunctional enzyme that catalyzes the rate-limiting step in sialic acid biosynthesis (8). All patients acquire the disease by autosomal recessive pattern and have at least one missense mutation in one allele, including the most common mutations V572L and M712T among Japanese and Iranian Jews, respectively. No patient with homozygous null mutation was identified. Genetically confirmed DMRV/hIBM diseases, initially recognized among Japanese and Iranian Jews (6,9–11), appear to afflict patients with diverse nationalities and cultural backgrounds (12–16).

The mechanism by which mutations in the *GNE* lead to the phenotype in DMRV/hIBM has remained unclear. We previously demonstrated that mutations in the *GNE* led to the reduction in either the UDP-GlcNAc 2-epimerase or ManNAc kinase activity (17); moreover, we have shown that myotubes from DMRV patients are hyposialylated, and this phenomenon can be corrected by the addition of free sialic acid and/or its precursor. Other groups have shown similar results regarding GNE activity, but in contrast, they suggested that only the cells derived from a patient carrying a homozygous epimerase mutation had a significant reduction in the overall membrane-bound sialic acid (18) and that *GNE* mutations may not contribute to alteration in sialylation in hIBM myoblasts (19). To address these issues, we developed a mouse model for the disease. In this paper, we present the first DMRV/hIBM mouse model that expressed only the mutated human *GNE* and show that this mouse evidently displays features of DMRV/hIBM seen in human patients.

RESULTS

Production of *Gne*$^{(-/-)}$h*GNE*D176V-Tg

The genomic configuration of the *Gne* gene and the targeting construct are shown in Figure 1A and B, respectively. The inserted Neo cassette replaced the 1.4 kb upstream of exon 3, exon 3 and 1.4 kb downstream of exon 3. With this strategy, only WT and *Gne*$^{(+/-)}$ mice were generated and no *Gne*$^{(-/-)}$ mouse was produced (data not shown), in concurrence with a previous report (20). We then proceeded to generate a transgenic mouse (h*GNE*D176V-Tg) that expressed the human mutated *GNE* with D176V, one of the most common *GNE* mutations in Japan, the structure of which is shown in Figure 1D. Of the resulting litters, nine mice were found to incorporate the h*GNE*D176V by polymerase chain reaction (PCR) analysis of genomic DNA isolated from tail snips, but only four lines were able to generate offspring. Using quantitative reverse transcriptase–polymerase chain reaction (RT–PCR), we quantified mRNA expression of h*GNE*D176V and endogenous *Gne* in muscle and other organs of these transgenic mice. Transgene expression was highest in the skeletal muscle, followed by heart, kidney, brain, spleen and liver (Fig. 2), whereas endogenous *Gne* expression was barely detected. We also determined the copy number using quantitative PCR by comparing the amplification of h*GNE*D176V with endogenous *Gne*. We calculated the copy numbers for lines 3, 6, 7 and 9 as 2, 4, 3 and 5, respectively. Consequently, we used this transgenic line 9 for producing the model mouse.

We crossed the h*GNE*D176V transgenic mouse with a *Gne*$^{(+/-)}$ to obtain a *Gne*$^{(+/-)}$h*GNE*D176V-Tg. Further, we crossed this *Gne*$^{(+/-)}$h*GNE*D176V-Tg with a *Gne*$^{(+/-)}$ to generate our model mouse, a transgenic mouse on a *Gne* knockout background, *Gne*$^{(-/-)}$h*GNE*D176V-Tg. Analysis of 823 newborn mice from independent heterozygous crosses indicated that the numbers of mice with the five genotypes, *Gne*$^{(-/-)}$h*GNE*D176V-Tg (+), *Gne*$^{(+/-)}$h*GNE*D176V-Tg(+), *Gne*$^{(+/-)}$h*GNE*D176V-Tg(−), *Gne*$^{(+/+)}$h*GNE*D176V-Tg(+) and *Gne*$^{(+/+)}$h*GNE*D176V-Tg(−) were 72 (9%), 225 (28%), 193 (24%), 177 (22%) and 136 (17%), respectively, almost approximating the expected ratio of Mendelian inheritance. Mice of the latter four genotypes did not demonstrate unusual phenotype and thus were considered as control littermates. Images for routine PCR for checking *Gne* genotype and the incorporation of the human *GNE*D176V are shown in Figure 1E, with the corresponding PCR fragments illustrated in A and C.

Hyposialylation is evident in the *Gne*$^{(-/-)}$h*GNE*D176V-Tg

Understandably, mutations in the *GNE* can affect sialylation of glycoconjugates because of the gene's role in sialic acid synthesis. We therefore measured the sialic acid levels in the *Gne*$^{(-/-)}$h*GNE*D176V-Tg mice using high-performance liquid chromatography (HPLC) with fluorometric detection. In wild-type (WT) mice, sialic acid levels are highest in the brain, followed by the liver, spleen and kidney (Fig. 3B, open boxes). In both skeletal and cardiac muscles, sialic acid levels are evidently lower than in other tissues. As we have expected, the total sialic acid in the *Gne*$^{(-/-)}$h*GNE*D176V-Tg mice are remarkably lower than WT. This hyposialylation is most remarkable in the serum (Fig. 3A). A significant reduction in total sialic acid level is seen in various tissues examined (Fig. 3B, closed boxes). We also measured sialic acid level in the h*GNE*D176V-Tg and noted that sialic acid levels are comparable to WT mice (Fig. 3B, gray boxes), although the transgenic expression was extremely higher than endogenous *GNE*.

Gne$^{(-/-)}$h*GNE* D176V-Tg has lower median of survival than littermate

The *Gne*$^{(-/-)}$h*GNE*D176V-Tg mice were indistinguishable from their littermates at birth and seemed healthy (Fig. 4A and B). After 30 weeks of age, these mice weighed less than their littermates (Fig. 4). Significant difference in weight is more pronounced and earlier in the female (Fig. 4C) compared

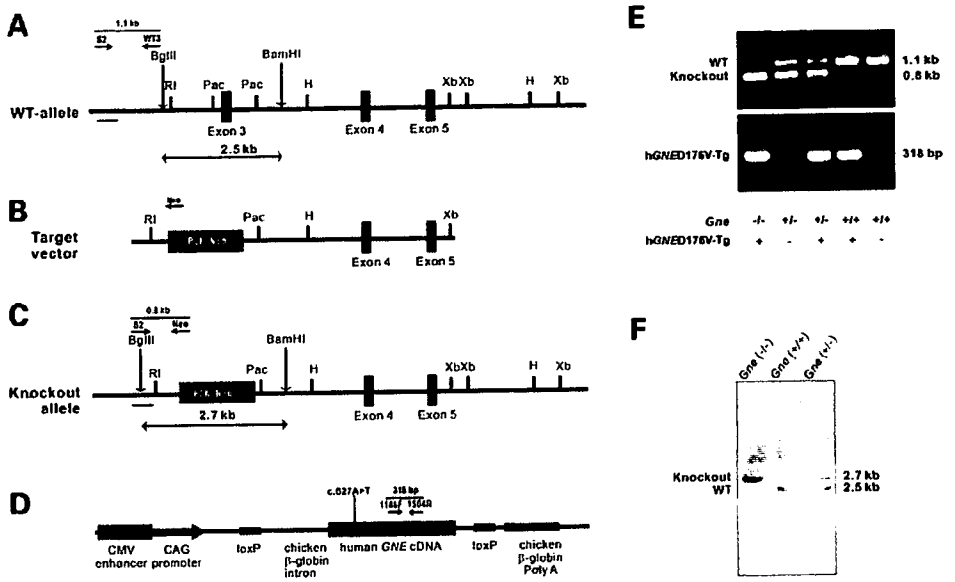

Figure 1. Genomic configuration of the *Gne* gene and the targeting vector. Schematic structure of the WT *Gne* gene (**A**), which contains exons 3, 4 and 5. Positions of restriction enzyme sites are shown. H, *Hin*dIII; Pac, *Pac*I; RI, *Eco*RI; Xb, *Xba*I. A 10.5 kb *Eco*RI–*Xba*I fragment was subcloned to make the targeting vector (**B**). One side of the Neo cassette was inserted 1.4 kb upstream of exon 3 and the other side of which was inserted 124 bp downstream of exon 3. In the knockout allele (**C**), the Neo cassette replaced the 1.4 kb upstream of exon 3, exon 3 and 124 bp downstream of exon 3. We selected homologous recombinants by neomycin resistance. (**D**) Structure of mutated human *GNE*D176V construct. CAG promoter was used to achieve expression in various tissues. (**E**) Genotyping of *Gne* and h*GNE*D176V-Tg mice by PCR. Five genotypes resulting from crossing a $Gne^{(+/-)}$h*GNE*D176V-Tg and $Gne^{(+/-)}$ are shown [from left to right: $Gne^{(-/-)}$h*GNE*D176V-Tg (+); $Gne^{(+/-)}$h*GNE*D176V-Tg(+); $Gne^{(+/-)}$h*GNE*D176V-Tg(−); $Gne^{(+/+)}$h*GNE*D176V-Tg(+); and $Gne^{(+/+)}$h*GNE*D176V-Tg(−)]. In *Gne* genotyping (upper panel), the 0.8 and 1.1 kb bands represent knockout and WT alleles, respectively (PCR products amplified by primer sets are illustrated in A and C). In h*GNE*D176V-Tg genotyping (lower panel), the presence of 318 bp band represents the integration of the h*GNE*D176V transgene. (**F**) Confirmation of *Gne* genotypes by Southern blot analysis. Tail genomic DNA were digested with *Bgl*II and *Bam*HI and analyzed by Southern blot analyses with 5′ probes as shown as bars in A and C. The fragments of 2.7 and 2.5 kb represent knockout and WT alleles, respectively.

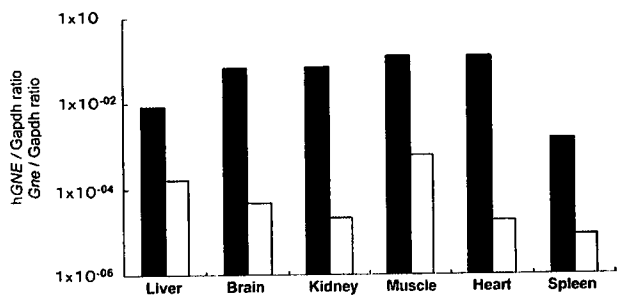

Figure 2. Expression of h*GNE*D176V (closed bars) and endogenous *Gne* (open bars) relative to Gapdh. Log values were used for computation of ratio. Highest expression of h*GNE*D176V is seen in skeletal and cardiac muscles, followed by heart, kidney, brain, liver and spleen.

to male mice (Fig. 4D). To investigate plausible explanations for this difference in weight, we performed gross inspection of the muscles and found out that some muscles, especially the gastrocnemius, were atrophic in the $Gne^{(-/-)}$h*GNE*D176V-Tg compared with control (Fig. 4E and F). This finding was more remarkable among females (Fig. 4E).

Surprisingly, the median survival rate was lower in the $Gne^{(-/-)}$ h*GNE*D176V-Tg as seen in Figure 4B. The cause of death could not be ascertained, but upon necropsy, no external gross abnormalities were seen and the internal organs appeared normal. On pathological examination, 5 out of 12 (41%) mice that died had RVs in the skeletal muscle; among these five mice, only one was before 40 weeks of age. Twenty-five percent had fibrosis and a few RVs in the diaphragm. Thirty-three had fibrosis in the cardiac muscles.

$Gne^{(-/-)}$h*GNE*D176V-Tg shows clinical phenotype

Using a tool for assessing general muscle strength, these mice notably performed worse than their littermates (Fig. 5A). Interestingly, a significant change in muscle power is noted after 30 weeks of age. We then proceeded to measure serum CK activity in the mice and found out that CK was significantly elevated in the $Gne^{(-/-)}$h*GNE*D176V-Tg mice when compared with their littermates (Fig. 5B), albeit the observation that these values are much lower compared with muscular dystrophy models such as $Large^{myd}$ and $Sgcb^{(-/-)}$ mice (data not shown). Because the appearance of phenotype seemed to be related to age, we measured CK activity according to different age groups. From Figure 5C, we note that elevation of CK activity starts at 30 weeks of age. Using gel electrophoresis, we verified that CK-MM isozyme was primarily increased (data not shown).

$Gne^{(-/-)}$h*GNE*D176V-Tg shows characteristic pathological features of DMRV

We checked whether the $Gne^{(-/-)}$h*GNE*D176V-Tg mice showed muscle phenotype not only by analysis of muscle power, but also by evaluating biopsy samples in five different

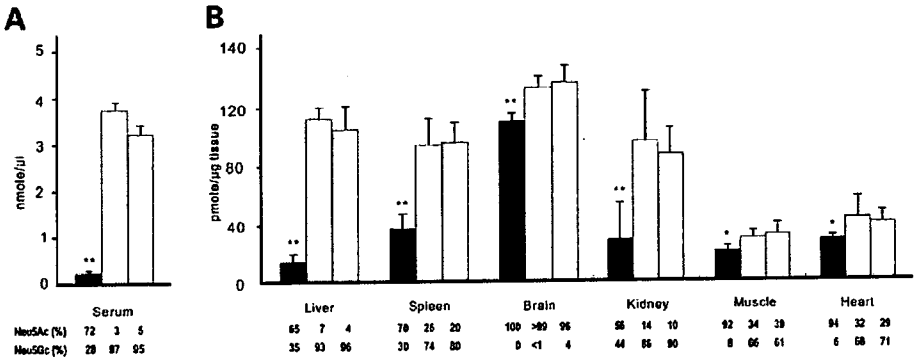

Figure 3. Measurement of total sialic acid in serum (A) and tissues (B) in $Gne^{(-/-)}$hGNED176V-Tg (closed bars), WT (open bars) and hGNED176V-Tg (gray bars); bars represent mean total sialic acid level, with standard deviation. Breakdown of sialic acid contents according to standards used (Neu5Ac and Neu5Gc) are shown below. Sialic acid levels of WT and hGNED176V-Tg are comparable. Note the reduction of sialic acid levels in the serum and tissues of the $Gne^{(-/-)}$h GNED176V-Tg mice. $^{*}P < 0.05$; $^{**}P < 0.005$.

age groups (10, 20, 30, 40 and 50 weeks). Morphometric analysis of the fibers in different age groups showed that the variation in fiber size become more marked with age, preferentially affecting the gastrocnemius and quadriceps muscles (data not shown); for this reason, we used the gastrocnemius muscle in further experiments. We found that at young age, they developed neither clinical nor pathological phenotype, as they were comparable with WT. Figure 6 A, D and G shows the representative sections from the $Gne^{(-/-)}$hGNED176V-Tg mice per age group. Histopathological analysis revealed almost normal findings in the muscle sections before 30 weeks of age (data not shown). In general, necrotic and regenerating processes are not observed in the young mice, although a few necrotic fibers are observed as they grow older. No endomysial or perimysial inflammation is seen.

Scattered small angular fibers are noted by 30 weeks of age (Fig. 6A), which is not seen in the littermates (Fig. 6B and C). The variation in fiber size becomes more noticeable as the mice grew older. In addition, fibers appear atrophic by 40 weeks of age, in support with the observation that the gastrocnemius muscle is relatively atrophic by gross inspection. Remarkably after 40 weeks, RVs are seen in scattered fibers (arrows in Fig. 6D and G). Occasionally, inclusion bodies are found in the fibers with or without RVs (arrowhead in Fig. 7A and B). Like in humans, these RVs are intensely stained with acid phosphatase, giving the impression that autophagic process is activated (Fig. 7C). We confirmed this by checking expression of lysosomal-associated membrane proteins (LAMPs) 1 and 2, and LC3 in muscle sections, all of which are upregulated. LAMP-1 is expressed predominantly within the vicinity of RVs (Fig. 7E). LAMP-2, on the other hand, is also expressed noticeably in the subsarcolemmal areas aside from its localization in the area of RVs (Fig. 7F). LC3 immunoreactivity is almost similar to LAMP-2, except that the perinuclear region is also highlighted (Fig. 7G).

Various proteins are expressed in the $Gne^{(-/-)}$hGNED176V-Tg muscles

One of the defining hallmark features of DMRV/hIBM is the presence of inclusion bodies that are presumed to have a role in muscle degeneration. These deposits have been shown to be immunoreactive to several proteins. Similar to human cases of DMRV, muscle cross-sections obtained from the $Gne^{(-/-)}$hGNED176V-Tg mice reveal positive Congo red staining (Fig. 7D), which is not observed in the myofibers of control mice (data not shown). Intense, demarcated signals are seen within the area of RVs and more frequently co-localizing with inclusion bodies which are often seen in DMRV/hIBM. As congophilia denotes deposition of proteins assuming a beta-pleated structure, we used the well-characterized 6E10, Aβ1-42, Aβ1-40 and A11 (β-amyloid oligomer), and β-site amyloid precursor protein-cleaving enzyme (BACE2) antibodies to check for intracellular accumulation of amyloid. Amyloid depositions occur within the myofibers and are seen to be occasionally associated with vacuolated fibers, as ~62% of RVs are positive for amyloid expression (data not shown). These amyloid inclusions are also noted in non-vacuolated fibers, including those which appear normal. β-Amyloid precursor protein (AβPP), which is recognized by 6E10 antibody (Fig. 7I), has intense, large, fairly demarcated immunoreactive signals within the RVs, similar to the staining pattern of the fibrillar forms of β-amyloid or β-amyloid peptides 1-42 and 1-40 (Fig. 7J and K). In good agreement with finding amyloid deposits in the myofibers, BACE2, which purportedly represents β-secretase activity, is upregulated in these myofibers and are seen as granular staining in the cytoplasm and intense immunoreactivity at subsarcolemmal areas (Fig. 7H). Interestingly, the oligomer form of β-amyloid, which is recognized by A11, is also expressed in the myofibers; positive signals are seen as aggregates around the RVs which are localized in areas distinct from fibrillar forms of amyloid (Fig. 7L).

We then analyzed skeletal muscles of mice from different age groups to see whether these amyloid accumulations are related to or can be considered as a function of age. We found out that these accumulations start to occur from 32 to 34 weeks of age, a period when virtually no RV is seen in the myofibers, and muscle pathology is characterized mainly by mild variation in fiber size (Fig. 8A and C). Both AβPP (Fig. 8B) and β-amyloid 1-42 peptide (Fig. 8D) show positive immunoreactivity within the myofibers.

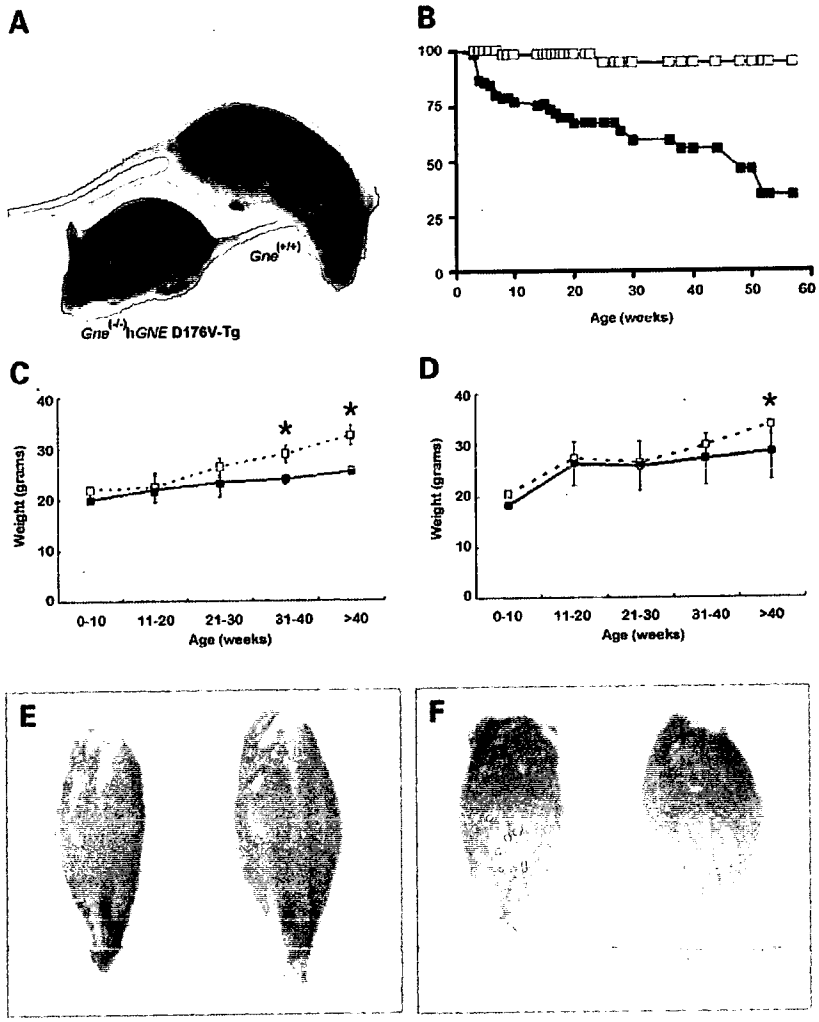

Figure 4. Overall phenotype of the $Gne^{(-/-)}$hGNED176V-Tg mice. (**A**) Picture of WT (up) and $Gne^{(-/-)}$hGNED176V-Tg (down) at 16 weeks of age. (**B**) Survival curve of mice: WT (open squares, $n = 71$ for males and females) and $Gne^{(-/-)}$hGNED176V-Tg mice (closed squares, $n = 71$ for males and females). $Gne^{(-/-)}$hGNED176V-Tg mice have significantly reduced life spans when compared with WT mice (log-rank test: $P = 0.001$). (**C**) Growth curves of female: WT (open squares, $n = 10$ per age group) and $Gne^{(-/-)}$hGNED176V-Tg mice (closed squares, $n = 10$ per age group). (**D**) Growth curves of male mice: WT (open squares, $n = 10$ per age group) and $Gne^{(-/-)}$hGNED176V-Tg (closed squares, $n = 10$ per age group). $Gne^{(-/-)}$hGNED176V-Tg mice have lower body weight after 30 weeks of age, and this is more pronounced in females; $^*P < 0.05$, Mann–Whitney test. Gastrocnemius muscles of female (**E**) and male (**F**) mice: $Gne^{(-/-)}$hGNED176V-Tg (left) and littermate (right). Atrophy is noted on gross inspection of hGNED176V-Tg gastrocnemius muscles; bar represents 5 mm.

The microtubule-associated protein tau, a cytoskeletal protein, has been shown to be abnormally phosphorylated and accumulated in DMRV and other muscle disorders (21–23). Similarly, in these $Gne^{(-/-)}$hGNED176V-Tg mice, these tau-positive deposits are evident as squiggly inclusion which are occasionally seen in vacuolated fibers (Fig. 7O).

SM-31, an antibody which detects neurofilaments, has been well characterized in DMRV/hIBM (21,24). In muscle sections, positive staining is seen within the vicinity of RVs (Fig. 7M); not all RVs, however, show immunoreactivity with this antibody. SM-310, on the other hand, only stains the intramuscular nerve bundles (Fig. 7N).

Because of the accumulation of several proteins in the myofibers, ER stress and the unfolded protein response (UPR) have been implicated in the pathogenesis of DMRV/hIBM. Using an antibody which recognizes one of the ER chaperones, we show that the UPR activation occurs in the $Gne^{(-/-)}$hGNED176V-Tg mice. Intracellular Grp-94 immunoreactivity is seen exclusively in vacuolated fibers (Fig. 7O). In the myofibers of the mice, strong reactivity to ubiquitin antibody in vacuolated and non-vacuolated fibers are seen (Fig. 7P), suggesting that the ubiquitin-proteosome system may as well be involved in the degradation of abnormal protein accumulations in the muscle and that misfolded proteins are ubiquitinated but not degraded.

Sarcolemmal proteins are also accumulated in DMRV/hIBM myofibers. Within the vicinity of the RVs, positive

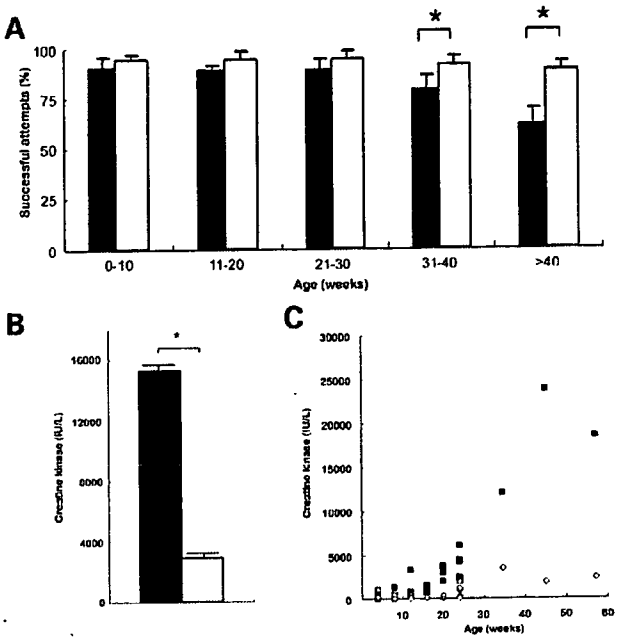

Figure 5. (A) Evaluation of overall motor strength using rod-climbing test, according to age group. Mean of three trials are shown. $Gne^{(-/-)}$ h*GNE*D176V-Tg mice (closed bars, $n = 10$) perform worse than littermates ($n = 10$). Significant difference is noticeable after 30 weeks of age. $^{*}P < 0.05$ (Mann–Whitney test). (B) Measurement of CK activity. Serum CK is significantly higher in $Gne^{(-/-)}$h*GNE*D176V-Tg mice (closed bars) compared with littermates (open bars). $^{*}P < 0.05$ (Students' *t*-test, two-tailed). (C) CK activity according to age. CK activity of $Gne^{(-/-)}$h*GNE*D176V-Tg mice (closed squares) starts to elevate after 30 weeks of age when compared with littermates (open diamonds).

α-dystroglycan (Fig. 7R), β-dystroglycan (Fig. 7S) and α-sarcoglycan (Fig. 7T) signals are observed.

In the myofibers of the control mice, no protein depositions were appreciated (data not shown).

Electron microscopic studies show evidence of autophagy and inclusions in the $Gne^{(-/-)}$h*GNE*D176V-Tg muscles

Ultrastructural studies confirm the activation of autophagy in $Gne^{(-/-)}$h*GNE*D176V-Tg muscles (Fig. 9). We obtained samples from a 42-week-old female mouse which had RVs as seen in light microscopy. In these samples, disorganization of myofibrils was seen in the vicinity of RVs. In about 500 myofibers examined, 10% showed ultrastructural evidence of autophagy. Collections of lysosomal autophagosomes containing undigested intracellular debris were seen, usually enclosed by a limiting membrane (Fig. 9A, arrow). The debris are often composed of light or electron-dense amorphous materials, and appeared like myelin whorls. Multiple, small, double-membrane-bound autophagic vacuoles were often contained within a larger autophagic vesicle (AV), suggesting that autophagy in these myofibers involves a continual process of AV consolidation (Fig. 9A, arrowhead). Multilamellar bodies are also observed (Fig. 9A, double arrows). Probable amyloid deposits are seen as amorphous and granular materials (Fig. 9B, magnified from Fig. 9A). Interestingly, ovoid and densely granular deposits, which may also be amyloid-like structures, are noted not only in the areas of autophagy (Fig. 9A, asterisk), but also in areas where myofibrillar architecture is well preserved (Fig. 9C). Occasionally, autophagic vacuoles are seen within the substance of these deposits (Fig. 9C, arrow).

$Gne^{(-/-)}$h*GNE*D176V-Tg shows pathological changes in the diaphragm and cardiac muscles

It has been a well-accepted fact that DMRV/hIBM primarily involved the skeletal muscles and that respiratory muscles are assumed to be spared as there had been no reports implying the involvement of the respiratory system. Interestingly, in the $Gne^{(-/-)}$h*GNE*D176V-Tg mice, we found that even diaphragm muscles are involved, although the findings range from almost normal findings to the presence of marked fibrosis and RVs in the myofibers (Fig. 10A). Likewise, we have observed inclusion bodies which are seen in both vacuolated and non-vacuolated fibers (data not shown).

It is now being recognized that some patients manifest with a variety of cardiac abnormalities, from the seemingly benign right bundle branch block to fatal arrhythmias. This led us to carefully check the status of cardiac muscles in the mice. We found out that few mice (around 20%) develop fibrosis in the cardiac tissue after the age of 30 weeks, and some show marked endomysial fibrosis (Fig. 10B). Moreover, amyloid deposition (Fig. 10C) and, occasionally, RVs (Fig. 10D) are also observed in cardiomyocytes. We also tried to functionally evaluate the heart by using 2D echocardiography and electrocardiogram, but we did not observe any abnormality pointing to definite cardiomyopathy or conduction defects (data not shown), although we only tested a limited number of mice.

DISCUSSION

Sialylation of oligosaccharide chains is a common and physiologically important event, and sialic acids are probably the most biologically important monosaccharide units of glycoconjugates. These negatively charged sugars at the terminal ends of glycoconjugates have very important biologic roles in mammalian development, and this is underscored by the embryonic lethality resulting from attempts to knockout *Gne* in the mice (20) and further supported by the absence of homozygous null mutations in humans. Making a transgenic *GNE* mouse on a *Gne* knockout background thus allowed us to rescue the phenotype in *Gne* knockout. Clearly, the $Gne^{(-/-)}$h*GNE*D176V-Tg resembles the phenotype in human DMRV/hIBM patients.

It is conceivable that a mutation in the *GNE*, a gene responsible for catalyzing the rate-limiting step in sialic acid biosynthesis, can lead to hyposialylation. Most, if not all, of the mutations causing DMRV caused partial reduction of the enzymatic activity of either UDP-GlcNAc 2-epimerase or ManNAc kinase of the *GNE* (17,19). As we have predicted, our results show that there is a marked reduction in sialic acid level, which can reflect *GNE* enzymatic activity, in the serum and other tissues of the $Gne^{(-/-)}$h*GNE*D176V-Tg mice.

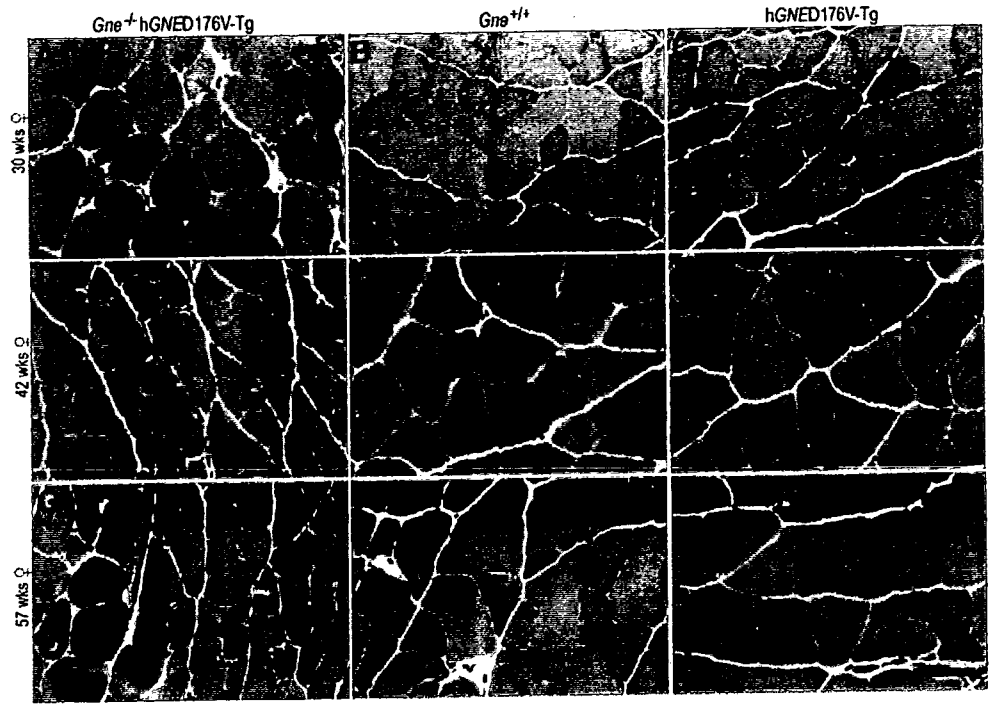

Figure 6. Hematoxylin and eosin sections from $Gne^{-/-}$hGNED176V-Tg (A, D, G), WT (B, E, H), hGNED176V-Tg (C, F, I). The hGNED176V-Tg mice are comparable to WT in all ages. In the $Gne^{-/-}$hGNED176V-Tg, there is a variation in fiber size which becomes more obvious as the mice aged. Fibrosis, necrotic or regenerating processes are not noted. Internalized nuclei are noted in scattered fibers. Small angular fibers are noted from around 30 weeks of age (A, arrows). Fibers with RVs (arrows) as well as cytoplasmic inclusions (arrowhead) are observed in scattered fibers from 42 weeks of age (D and G). Bar represents 40 μm.

With regards to expression of *GNE* in various tissues, it has been shown that expression in the muscle is very low (25). Our results show, on the other hand, that mRNA expression of h*GNE* D176V-Tg is highest in the muscle, and we attribute this to the promoter that we used in the transgene construct. Previously, we have shown that using CAG promoter efficiently promotes expression of a gene into adult skeletal muscles (26).

Skeletal muscle is exclusively affected in DMRV/hIBM, although it is reasonable to expect multi-organ involvement because of the ubiquitous expression of *GNE*. In our mice, the skeletal muscle is clearly affected despite the data that hyposialylation is not that remarkable compared with other organs. Our results suggest that even a slight reduction in sialic acid level can cause symptoms in skeletal muscles; however, the selectivity of skeletal muscle may not be explained by the *Gne* expression levels and sialic acid levels in each organ.

It is notable that some of the $Gne^{-/-}$hGNED176V-Tg mice die sooner than their littermates, but the precise reason for this is not known at present. It is, however, evident that a significant number of the autopsied mice showed pathological findings in the diaphragm and the heart. In humans, there was a report on two siblings with the homozygous D176V mutation who died from arrhythmia (27), but there had been no reports on respiratory involvement among patients.

The onset of symptoms among DMRV patients has been reported to be from the second to the third decade (3), although there are a few anecdotal reports of early onset (28). Interestingly in the $Gne^{-/-}$hGNED176V-Tg mice, the onset of clinical phenotype is noted around 30 weeks of age, which can be considered to be similar to that in humans, using lifespan and ability to reproduce for points of comparison. It is peculiar that gastrocnemius and quadriceps muscles are preferentially involved in the mice, whereas in humans, the tibialis anterior is remarkably involved while the quadriceps are affected relatively late in the course of the disease. In our recent data on the clinical presentation of DMRV, however, it is clear that the gastrocnemius can be affected more severely in some cases (28).

We tried to check fiber-type involvement in these muscles and found out that both slow and fast fibers are affected in human and mice, in terms of the presence of RVs, but fast-type fibers are predominantly involved (data not shown). Sporadic IBM has some pathologic similarities with DMRV; recently, it has been shown that the presence of inclusions on routine histochemistry and the pathogenic accumulation of β-amyloid protein occur in fast twitch muscles, both in a transgenic model of IBM and in IBM patients (29), implying that fast-type fibers are more vulnerable to pathologic changes. Further analysis is needed on this aspect to derive a more conclusive data.

CK levels are reported to be mildly or moderately elevated in patients, although there were isolated cases where the CK activity was above 1000 IU/l (11). CK elevation has always been correlated with the presence of necrotic and regenerating processes in the skeletal muscle, but which are only

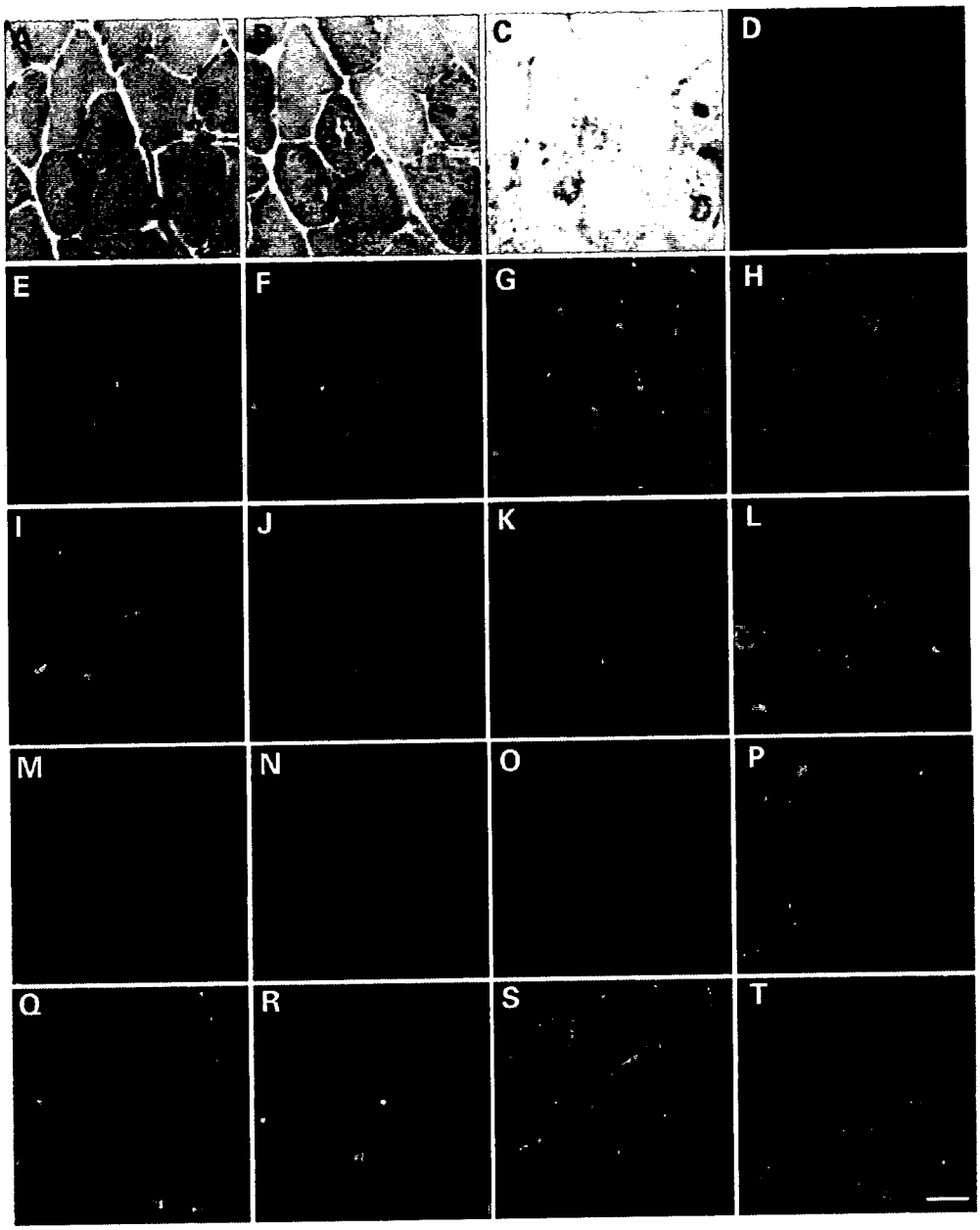

Figure 7. Serial sections taken from a 42-week-old female *Gne*$^{-/-}$ hGNED176V-Tg mouse. (**A**) Hematoxylin and eosin sections showing fibers with RVs and cytoplasmic inclusions. (**B**) In modified Gomori trichrome, vacuoles are rimmed by eosinophilic granules. (**C**) Acid phosphatase activity is enhanced around RVs, suggesting upregulation of lysosomal activity in these areas. (**D**) Congo red staining visualized by Texas red filters shows positive staining in fibers with or without RVs, and appear as large, granular deposits. Immunoreactivity to lysosomal proteins confirm the presence of autophagy in fibers with RVs: (**E**) LAMP-1 signals are seen in the areas of RVs; (**F**) LAMP-2 has subsarcolemmal immunoreactivity, in addition to positive staining in RVs; (**G**) LC3 stains the same areas as LAMP-2, in addition to perinuclear areas. Intracellular deposition of amyloid is seen in vacuolated or non-vacuolated fibers: (**H**) Increased reactivity to BACE2 is seen in cytoplasm of fibers with RVs and within the vicinity of RVs; (**I**) AβPP expression is intense in area of RVs, seen as discrete deposits; (**J**) β-amyloid 1-42 and (**K**) β-amyloid 1-40 stainings are likewise seen as discrete deposits within the vicinity of RVs; (**L**) β-amyloid oligomeric antibody signals are noted as aggregates of small granule-like deposits around the RVs. Neurofilament deposition is observed in the myofibers: SM-31 (**M**) immunoreactivity is occasionally noted within the vicinity of RVs, whereas SM-310 (**N**) only stains intramuscular nerve bundles. (**O**) Epitopes of phosphorylated tau are observed in some fibers with RVs. (**P**) Fibers with RVs have intense ubiquitin staining around RVs and granule-like signals in these fibers. (**Q**) Grp94, an endoplastic reticulum luminal stress protein, is upregulated exclusively in vacuolated fibers as large granular deposits within the RVs. Sarcolemmal proteins are deposited within the vicinity of RVs: (**R**) α-dystroglycan; (**S**) β-dystroglycan; and (**T**) α-sarcoglycan. Bar represents 20 μm.

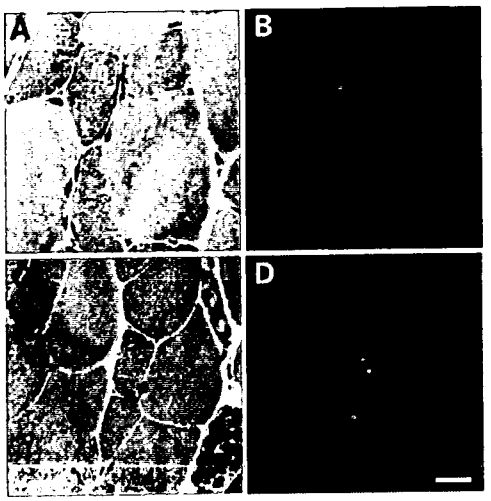

Figure 8. Amyloid deposition precedes RV formation. Sections taken from the gastrocnemius of a 34-week-old female mouse shows variation in fiber size in hematoxylin and eosin sections (A and C). Note the absence of RVs or cytoplasmic inclusions in these fibers. Amyloid depositions are seen as immunofluorescent signals in small fibers (B, β-amyloid 1-42; D, AβPP). Bar represents 20 μm.

Figure 9. Ultrastructural evidence of autophagy and intracellular inclusions. (A) Collections of lysosomal autophagosomes with intracellular debris which are light or electron-dense amorphous materials enclosed by a limiting membrane (arrow). Multilamellar structures are also observed (double arrows). Ovoid and dense deposits which are probably amyloid deposits are likewise seen (asterisk). (B) Probable amyloid deposits are seen as amorphous and granular material surrounded by autophagosomes (B, magnified from A). (C) Dense, granular deposits, which are probably amyloid accumulations, are also noted in areas where architecture of myofibrils are generally well preserved; occasionally, autophagic vacuoles are seen within the substance of these deposits (arrow). Bar represents 2 μm.

occasionally found in DMRV/hIBM. Elevation of serum CK is also seen in the $Gne^{(-/-)}$h*GNE*D176V-Tg mice, although necrotic and regenerating processes are barely detectable. Our data suggest that there might be other mechanisms which trigger CK release into the circulation, aside from myonecrosis. It has not been clarified if CK release into the blood stream may be induced by deglycosylation of membrane proteins, although some studies suggested that removal of sialic acids by neuraminidase treatment may influence sarcolemmal permeability (30). Further tests are clearly needed to shed some insight on the CK elevation in DMRV/hIBM and $Gne^{(-/-)}$h*GNE*D176V-Tg mice.

A subject of poignant interest is whether RV formation, one of the hallmarks of DMRV/hIBM, is the primary event that induces muscle fiber atrophy and loss, notwithstanding the fact that RVs are nonspecific and could be seen in a multitude of myopathies. In the $Gne^{(-/-)}$h*GNE*D176V-Tg mice, weakness is clearly noted before the occurrence of RVs, implying that other factors should be responsible for the earlier onset of weakness. Consistently, we have documented that serum and other tissues are hyposialylated, and this phenomenon is not at all correlated with age, strongly suggesting that hyposialylation may play a role in the development of clinical manifestations exhibited by patients. Previous studies have implicated that sialic acid directly contributes to the negative surface potential of cells, because desialylation of rat skeletal muscle sodium channel leads to reduced sensitivity of these channels to the effects of external calcium (31). This would mean that voltage gating parameters are shifted to the point that channels required a larger depolarization in order to gate, which may suggest that the mechanism of weakness may be due to the reduced excitability of the muscle membrane as a result of sodium channel desialylation.

The hallmarks of DMRV/hIBM include RVs that are autophagic in nature (32) and cytoplasmic inclusions in vacuolated and non-vacuolated fibers, both of which are seen in muscle sections from the $Gne^{(-/-)}$h*GNE*D176V-Tg mice. Several proteins have been shown to accumulate in DMRV myofibers (33,34), and most of which have been demonstrated to be mainly associated with amyloid because of the positive reactivity to crystal violet and Congo red, suggesting that they assume the beta-pleated-sheet configuration. In general, more than 20 unrelated proteins, including β-amyloid (34), prion, tau (21) and transthyretin, can abnormally unfold and self-aggregate to form beta-pleated-sheet amyloid (35). The association of these proteins with DMRV/hIBM pathomechanism has largely been enigmatic up to this time, but unfolding and misfolding of proteins most probably play a role. Previous reports have alluded to the role of sialic acid in proper folding of proteins (35-37). The ultimate fate of aggregated, misfolded glycoproteins is degradation, hence the activation of UPR is expected, which could explain the presence of ubiquitin signals in the myofibers of the $Gne^{(-/-)}$h*GNE*D176V-Tg mice and upregulation of ubiquitin and proteasome in DMRV/hIBM myofibers (38).

The implication of amyloid deposition in the formation of RVs in both DMRV/hIBM and s-IBM (39) is supported by our finding that the occurrence of amyloid inclusions in the myofibers preceded RV formation. Amyloid itself has been shown *in vitro* to block the degradation of ubiquitinated

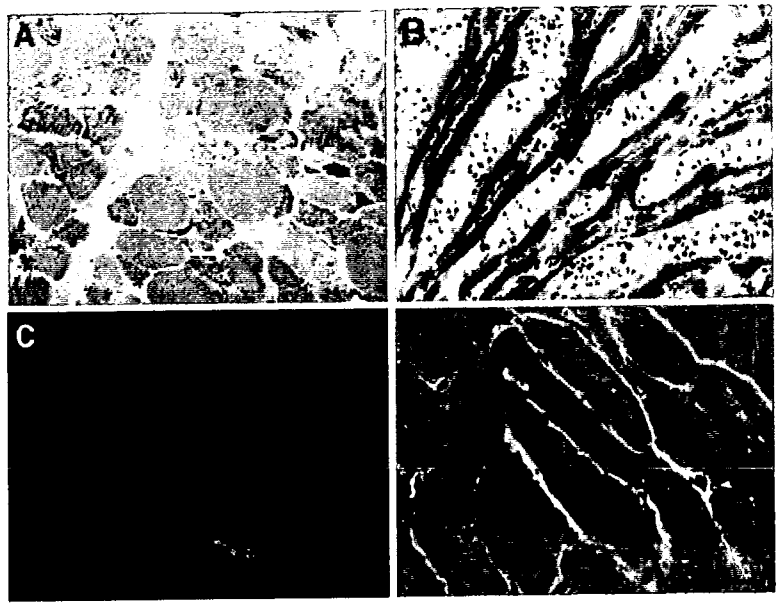

Figure 10. The diaphragm and cardiac muscles are likewise involved in the $Gne^{(-/-)}$hGNED176V-Tg mice. (**A**) Modified Gomori trichrome section of a 48-week-old male $Gne^{(-/-)}$hGNED176V-Tg. Note the presence of endomysial fibrosis and fiber with RV. (**B**) Hematoxylin and eosin sections from a 54-week-old female $Gne^{(-/-)}$hGNED176V-Tg showing marked fibrosis. (**C**) Amyloid deposition (β-amyloid 1-42) is seen in the cardiomyocytes of the same mouse in (B). (**D**) HE section of cardiac muscle from a 42-week-old male $Gne^{(-/-)}$hGNED176V-Tg reveals that RVs are occasionally seen in cardiomyocytes.

proteins by inhibiting proteasome activity (40) hence its accumulation may not only lead to cytotoxicity, but also may further aggravate protein misfolding. In addition, it has been clarified that overproduction of amyloid can induce tau hyperphosphorylation and decrease its solubility (41). Sialylation and glycosylation of amyloid precursor protein, which contains both *O*- and *N*-glycans, appear to be important for its proteolytic processing, secretion and metabolism (42–45). Interference with the formation of *N*-linked glycans resulted in a decrease in secreted AβPP and an increase in the level of the cellular form of the protein, which has a higher propensity to form β-amyloid peptide (42,46). Although amyloid fibrils have been considered to be cytotoxic, there is current experimental evidence that pre-amyloid oligomeric complexes or aggregates, either diffusely occurring or in a protofibril stage, can be very cytotoxic (47). The presence of dense deposits in areas with relatively preserved myofibrillar architecture on electron microscopy strongly suggest that deposition of amyloid and amyloid-like structures pre-date RV formation.

Because DMRV/hIBM patients do not present, in general, with symptoms reflecting involvement of the respiratory system, it is assumed that the diaphragm is relatively spared in this myopathy. In the $Gne^{(-/-)}$hGNED176V-Tg mice, it is clear that the diaphragm can be involved, despite the absence of overt respiratory difficulties. The presence of pathological findings in the sacrificed mice, not only in the ones that died suddenly, may suggest that the presence of RVs *per se* may not correlate to severity in phenotype with respect to involvement of diaphragm. A more sensitive method of assessing the respiratory status of these mice, vis-à-vis a plain observation, might be helpful in clarifying the extent to which respiratory system is involved. Our results suggest that careful evaluation of respiratory and cardiovascular functions is logical and warranted in human patients.

In the $Gne^{(-/-)}$hGNED176V-Tg mice, we have seen RVs in the cardiac muscles obtained from a couple of mice, clearly supporting the presence of cardiac involvement in DMRV/hIBM. It has always been reported that DMRV involves primarily skeletal muscles but recently, however, it is being recognized that other organs may likewise be involved. For example, cardiac involvement is not very rare as it is seen in 18% of patients, with a spectrum of manifestations ranging from an incomplete right bundle branch block to a fatal arrhythmia which led to sudden death (25,26). Sialic acid was shown to be an important component on the surface of the heart muscle cells, because its removal reduced the cell surface negative charge by 25% (48) and produced a large increase in cardiac myocyte Ca^{2+}, followed by marked cell contracture (49), emphasizing the importance of negatively charged sialic acid-containing gangliosides in the maintenance of cardiac cell physiological Ca^{2+} permeability. More importantly, it has been demonstrated that in myocardial cells, desialylation of cells by neuraminidase treatment causes aberrant electrical activity (50) and may lead to arrhythmia (51).

In conclusion, we have generated the first mouse model of DMRV/hIBM, which resembles the clinical, pathological and biochemical features of the disease in humans. The $Gne^{(-/-)}$hGNED176V-Tg mouse is a concrete evidence that mutations in the *GNE* are causative of DMRV/hIBM. Indeed, these DMRV/hIBM mice will be a valuable tool to

search for further clues in unraveling the pathomechanism of this myopathy. As we have clearly documented in these mice, hyposialylation plays a key role in the pathogenesis of DMRV/hIBM and is of paramount importance in considering therapeutic trials.

METHODS

Generation of *Gne* knockout mice

The *Gne* knockout mice ($Gne^{(-/-)}$) was produced in inGenious Targeting Laboratory (New York, NY, USA). The 17 kb mouse genomic DNA fragment, containing exons 3, 4 and 5, was cloned from the mouse 129Sv/Ev lambda genomic library. The Neo cassette that was inserted replaced the 1.4 kb upstream of exon 3, exon 3 and 124 bp downstream of exon 3 (Fig. 1). The resulting targeting vector was linearized by *Not*I, purified and then transfected by electroporation into ES cells. Positive clones after neomycin selections were identified using PCR (primer sequences available upon request).

Generation of h*GNE*D176V-Tg

The cDNA for *GNE* mutant was obtained by reverse-transcribed PCR from skeletal muscle RNA of a DMRV patient with the D176V mutation and cloned into pCR-Blunt vector (Invitrogen, Carlsbad, CA, USA) as described previously (17). Cloned cDNA was sequenced by ABI cycle-sequencing procedures using an ABI 3100 (Applied Biosystems, Foster City, CA, USA). The *Xho*I fragment containing *GNE* mutant cDNA was excised and inserted into pCAGGS vector in which gene expression is driven by a CAG promoter (52). *loxP* sequences were introduced to flank the cDNA insert. *Sal*I fragment was purified and injected into C57BL/6 oocytes and subsequently transplanted into recipient mice. Founders were bred to WT C57BL/6 females to check for germline transmission, which was confirmed by PCR analyses on genomic DNA.

Production of $Gne^{(-/-)}$h*GNE*D176V-Tg

To maintain the same copy number of transgene, stringent measures were taken in generating mice. The h*GNE*D176V-Tg mouse was crossbred to *Gne* heterozygous mouse ($Gne^{(+/-)}$) to create a $Gne^{(+/-)}$ mouse that carried the human *GNE* ($Gne^{(+/-)}$h*GNE*D176V-Tg). The latter was then mated with a $Gne^{(+/-)}$ mouse, to obtain a mouse that harbors the human D176V mutated *GNE* in a *Gne* knockout background.

For genotyping, DNA was isolated from mouse tails. *Gne* mice genotyping was carried out using PCR analysis on tail genomic DNA with the following primers: Neo, WT3 and S2 (primer sequences available upon request). Further, DNA was digested with *Bam*HI, subjected to Southern blotting, and then analyzed by hybridization to a 500 bp probe.

For transgenic mice, the following oligonucleotides were used to amplify a 318 bp segment found specifically in human *GNE*: 1186F, CTTCAAGAGCCACTGCAAA; 1504R, CAATTCCTTCCCGAGGATT.

mRNA expression and determination of copy number

Mouse skeletal muscles, heart, brain, spleen and liver were dissected and rapidly frozen in liquid nitrogen. Total RNA was extracted from cryostat sections of tissues with TRIzol (Invitrogen) following the manufacturer's protocol. Single-strand cDNA was synthesized from RNA by reverse transcription using the Superscript RNase H^- Reverse Transcriptase (Invitrogen) and random hexamers. Gene expression was measured by quantitative real-time PCR in i-Cycler IQ system (Bio-Rad Laboratories, Hercules, CA, USA). Primers (1186F and 1504R) were used to span exon–intron junctions to prevent amplification of genomic DNA. Relative quantification of gene expression was determined by comparison of threshold values as suggested by the manufacturers. All results were normalized with respect to Gapdh expression.

Transgene copy number was determined by the i-Cycler IQ system using the SYBR Green reagent kit according to the manufacturer's instructions. Triplicate samples of tail DNA from transgenic mice of each line were analyzed concurrently against a standard curve of scaled concentrations of an external standard. Primers were designed to amplify the transgene h*GNE*D176V and endogenous *Gne*; twice the ratio of the h*GNE*D176V/*Gne* amplicons was interpreted as copy number.

Sialic acid measurement

The bound sialic acids from the serum and pieces of different tissues were released using 20 mM sulfuric acid hydrolysis for 1 h at 80°C. Free sialic acids were then derivatized with 1,2-diamino-4,5-methylenedioxybenzene and analyzed with reversed-phase HPLC fluorescence detection as described previously (53). The eluant was monitored by fluorescence and measured by comparison with Neu5Ac and Neu5Gc standards (from 0.05 to 5 nmol/μl). Total protein from tissues was measured using the Bio-Rad Protein Assay (Bio-Rad Laboratories) according to the manufacturer's protocol.

General assessment for motor strength and fatigability

Whole-animal strength and fatigability were measured according to a test procedure (here referred to as rod-climbing test) previously reported (54). In brief, this test required the mice to pull themselves on top of a suspended rod (3 mM in diameter). The measurement of muscle weakness was based on the mean percentage of passes over 15 trials of the test in a 3-min period. Fatigability was assessed as the average pass rate over time for each group of mice. The test was repeated at least three times after a 2-week period.

Histopathological and histochemical analyses

Fresh specimens from individual skeletal and cardiac muscles were snap-frozen in liquid-nitrogen-cooled isopentane and stored at −80°C until further processing. We stained frozen sections (6 μm) of transversal skeletal and cardiac muscles with a battery of histochemical stains including hematoxylin and eosin, modified Gomori trichrome and acid phosphatase. Sections were analyzed by light microscopy. We performed Congo red staining in 10 μm cryosections following the

Table 1. Antibodies used in the study

Antibody	Manufacturer	Type	Dilution
AβPP (6E10)	Chemicon International, Inc., Temecula, CA	Mouse monoclonal	1:1000
Aβ 1-40	Chemicon	Rabbit polyclonal	1:100
Aβ 1-42	Chemicon	Rabbit polyclonal	1:100
Aβ oligomer (A11)	Chemicon	Rabbit polyclonal	1:1000
Human Beta Site APP cleaving enzyme	Alpha Diagnostic International	Rabbit polyclonal	1:100
Caveolin 3	Transduction Laboratories, Lexington, KY	Rabbit polyclonal	1:400
α-Dystroglycan (VIA4-1)	Upstate Cell Signaling Solutions, Lake Placid, NY	Mouse monoclonal	1:100
β-Dystroglycan	A gift from Dr Ejiro Ozawa	Rabbit polyclonal	1:200
Grp94 (9G10)	Stressgen Biotechnologies, Calgary, Canada	Rat monoclonal	1:30
LAMP-1 (25)	BD Transduction Laboratories, Lexington, KY	Mouse monoclonal	1:100
LAMP-2A	A gift from Dr Fumitaka Oyama	Rabbit polyclonal	1:100
LC3	A gift from Dr Tamotsu Yoshimori	Rabbit polyclonal	1:200
NCAM (123C3)	Santa Cruz Biotechnology, Inc.	Mouse monoclonal	1:100
α-Sarcoglycan (Ad1/20A6)	Novocastra Laboratories, Ltd	Mouse monoclonal	1:100
β-Sarcoglycan (βSarc/5B1)	Novocastra Laboratories, Ltd	Mouse monoclonal	1:100
Poly-ubiquitin (FK1)	Biomol International	Mouse monoclonal	1:500
Neurofilament (SM-31)	Sternberg Monoclonals, Inc., Maryland, USA	Mouse monoclonal	1:1000
Neurofilament (SM-310)	Sternberg Monoclonals, Inc., Maryland, USA	Mouse monoclonal	1:1000
tau C	A gift from Dr Fumitaka Oyama	Rabbit polyclonal	1:1000

Putchler's modification, and viewed sections under light microscope and conventional fluorescence microscope using Texas-red filters (39). For immunohistochemical analysis, tissue sections were fixed either in acetone or paraformaldehyde, depending on the primary antibody used, and blocked with 5% normal serum and 2% bovine serum albumin in phosphate-buffered saline. The primary antibodies used are listed in Table 1. We used several antibodies which recognize β-amyloid. 6E10, which is a human-specific antibody but also reacts to murine tissue when the amyloid burden is high, primarily recognizes AβPP (residues 1–16) after α-secretase cleavage. It also recognizes, in addition, C99 fragment and β-amyloid peptides (1-40 and 1-42) which have been shown to be prone to aggregation. The anti-oligomeric antibody (A11) is specific to the oligomeric structure of β-amyloid peptides. The following secondary antibodies were used appropriately: anti-goat IgG F (ab')-2-fragment, FITC-conjugated (EY Laboratories, San Mateo, CA, USA); anti-rabbit IgG (H + L), Alexa Fluor-conjugated (Molecular Probes, Eugene, OR, USA); anti-mouse IgG1, FITC-conjugated (Sanbio/Monosan, Uden, The Netherlands). Images were collected and analyzed with a laser scanning microscope (Olympus, Tokyo, Japan) with its appropriate software.

Morphometric analysis of fibers

Muscle cross-sections were stained with rabbit polyclonal antibody against caveolin 3 followed by a fluorescent secondary antibody. Digital images from fluorescence signals were observed under a confocal microscope and the widest diameter was recorded for 600 or more fibers using Image-J software from the public domain NIH Image program (developed at the US National Institutes of Health and available on the Internet at http://rsb.info.nih.gov/nih-image/). Results were analyzed using Statistical Software for Social Sciences (SPSS for Windows, Rel. 11.0.0., 2001, SPSS, Inc., Chicago, IL, USA) software.

Electron microscopy

The muscle specimens were immediately fixed for 2 h in 2.5% cold glutaraldehyde with 0.1 M cacodylate buffer, pH 7.3. After washing in cacodylate buffer, the specimens were post-fixed in 1% osmium tetroxide in the same buffer, dehydrated with graded series of ethanol and embedded in Epon. Semi-thin sections (0.5 μm) were stained with toluidine blue alkaline. Ultrathin sections were stained with uranyl acetate, citrated and observed with an H-600 electron microscope (Hitachi, Tokyo, Japan) at 75 kV.

Serum creatine kinase

Blood samples were obtained either by inferior vena cava aspiration or careful collection from mouse tail. Total CK activity was measured by a spectrophotometric assay employing a commercial kit (CPK-L Determiner, Kyowa MEDEX, Tokyo, Japan). For confirmation, CK isoforms are electrophoretically analyzed by using Titan Gel CK Isozyme kit (Helena Laboratories, Beaumont, TX, USA) following the manufacturer's protocol.

Statistical analysis

Data were entered into SPSS version 11.0 and were analyzed by computation of the frequency and the mean ± standard deviation (SD) and/or percentage. The data were then subjected to a univariate analysis (Fisher's exact test), Students' *t*-test, Wilcoxon paired test, ANOVA, or Mann-Whitney test, log-rank test or multiple regression analysis, whichever was appropriate. *P*-values less than 0.05 were considered to be statistically significant.

ACKNOWLEDGEMENTS

The authors thank Yoko Keira, Genri Kawahara, Mari Okada and Kumiko Murayama for their invaluable support and assistance.

FUNDING

Funding for the Open Access publication charge was obtained from the 'Research on Psychiatric and Neurological Diseases and Mental Health' from Health and Labour Sciences Research Grants; the 'Research on Health Sciences focusing on Drug Innovation' from the Japanese Health Sciences Foundation; the 'Research Grant (16B-2, 17A-10) for Nervous and Mental Disorders' from the Ministry of Health, Labour and Welfare; and the Program for Promotion of Fundamental Studies in Health Sciences of the National Institute of Biomedical Innovation (NIBIO); and Neuromuscular Disease Foundation.

Conflict of Interest statement. None.

REFERENCES

1. Nonaka, I., Sunohara, N., Ishiura, S. and Satoyoshi, E. (1981) Familial distal myopathy with rimmed vacuole and lamellar (myeloid) body formation. *J. Neurol. Sci.*, **51**, 141–155.
2. Argov, Z. and Yarom, R. (1984) 'Rimmed vacuole myopathy' sparing the quadriceps: a unique disorder in Iranian Jews. *J. Neurol. Sci.*, **64**, 33–43.
3. Nonaka, I., Noguchi, S. and Nishino, I. (2005) Distal myopathy with rimmed vacuoles and hereditary inclusion body myopathy. *Curr. Neurol. Neurosci. Rep.*, **5**, 61–65.
4. Ikeuchi, T., Asaka, T., Saito, M., Tanaka, H., Higuchi, S., Tanaka, K., Saida, K., Uyama, E., Mizusawa, H., Fukuhara, N. *et al.* (1997) Gene locus for autosomal recessive distal myopathy with rimmed vacuoles maps to chromosome 9. *Ann. Neurol.*, **41**, 432–437.
5. Mitrani-Rosenbaum, S., Argov, Z., Blumenfeld, A., Seidman, C.E. and Seidman, J.G. (1996) Hereditary inclusion body myopathy maps to chromosome 9p1-q1. *Hum. Mol. Genet.*, **5**, 159–163.
6. Nishino, I., Noguchi, S., Murayama, K., Driss, A., Sugie, K., Oya, Y., Nagata, T., Chida, K., Takahashi, T., Takusa, Y. *et al.* (2002) Distal myopathy with rimmed vacuoles is allelic to hereditary inclusion body myopathy. *Neurology*, **59**, 1689–1693.
7. Eisenberg, I., Avidan, N., Potikha, T., Hochner, H., Chen, M., Olender, T., Barash, M., Shemesh, M., Sadeh, M., Grabov-Nardini, G. *et al.* (2001) The UDP-*N*-acetylglucosamine 2-epimerase/*N*-acetylmannosamine kinase gene is mutated in recessive hereditary inclusion body myopathy. *Nat. Genet.*, **29**, 83–87.
8. Keppler, T., Hinderlich, S., Langner, J., Sewartz-Albiez, R., Reutter, W. and Pawlita, M. (1999) UDP-GlcNAc 2-epimerase: a regulator of cell surface sialylation. *Science*, **284**, 1372–1376.
9. Eisenberg, I., Grabov-Nardini, G., Hochner, H., Korner, M., Sadeh, M., Bertorini, T., Bushby, K., Castellan, C., Felice, K., Mendell, J. *et al.* (2003) Mutations spectrum of GNE in hereditary inclusion body myopathy sparing the quadriceps. *Hum. Mutat.*, **21**, 99.
10. Argov, Z., Eisenberg, I., Grabov-Nardini, G., Sadeh, M., Wirguin, I., Soffer, D. and Mitrani-Rosenbaum, S. (2003) Hereditary inclusion body myopathy: the Middle Eastern genetic cluster. *Neurology*, **60**, 1519–1523.
11. Tomimitsu, H., Shimizu, J., Ishikawa, K., Ohkoshi, N., Kanazawa, I. and Mizusawa, H. (2004) Distal myopathy with rimmed vacuoles (DMRV): new GNE mutations and splice variant. *Neurology*, **62**, 1607–1610.
12. Kim, B.J., Ki, C.S., Kim, J.W., Sung, D.H., Choi, Y.C. and Kim, S.H. (2006) Mutation analysis of the GNE gene in Korean patients with distal myopathy with rimmed vacuoles. *J. Hum. Genet.*, **51**, 137–140.
13. Ro, L.S., Lee-Chen, G.J., Wu, Y.R., Lee, M., Hsu, P.Y. and Chen, C.M. (2005) Phenotypic variability in a Chinese family with rimmed vacuolar distal myopathy. *J. Neurol. Neurosurg. Psychiatry*, **76**, 752–755.
14. Broccolini, A., Ricci, E., Cassandrini, D., Gliubizzi, C., Bruno, C., Tonoli, E., Silvestri, G., Pescatori, M., Rodolico, C., Sinicropi, S. *et al.* (2004) Novel GNE mutations in Italian families with autosomal recessive hereditary inclusion-body myopathy. *Hum. Mutat.*, **23**, 632.
15. Liewluck, T., Pho-Iam, T., Limwongse, C., Thongnoppakhun, W., Boonyapisit, K., Raksadawan, N., Murayama, K., Hayashi, Y.K., Nishino, I. and Sangruchi, T. (2006) Mutation analysis of the GNE gene in distal myopathy with rimmed vacuoles (DMRV) patients in Thailand. *Muscle Nerve*, **34**, 775–778.
16. Amouri, R., Driss, A., Murayama, K., Kefi, M., Nishino, I. and Hentati, F. (2005) Allelic heterogeneity of GNE gene mutation in two Tunisian families with autosomal recessive inclusion body myopathy. *Neuromuscul. Disord.*, **15**, 361–363.
17. Noguchi, S., Keira, Y., Murayama, K., Ogawa, M., Fujita, M., Kawahara, G., Oya, Y., Imazawa, M., Goto, Y., Hayashi, Y.K. *et al.* (2004) Reduction of UDP-*N*-acetylglucosamine 2-epimerase/*N*-acetylmannosamine kinase activity and sialylation in distal myopathy with rimmed vacuoles. *J. Biol. Chem.*, **279**, 11402–11407.
18. Salama, I., Hinderlich, S., Shlomai, Z., Eisenberg, I., Krause, S., Yarema, K., Argov, Z., Lochmuller, H., Reutter, W., Dabby, R. *et al.* (2005) No overall hyposialylation in hereditary inclusion body myopathy myoblasts carrying the homozygous M712T GNE mutation. *Biochem. Biophys. Res. Commun.*, **328**, 221–226.
19. Hinderlich, S., Salama, I., Eisenberg, I., Potikha, T., Mantey, L.R., Yarema, K.J., Horstkorte, R., Argov, Z., Sadeh, M., Reutter, W. *et al.* (2004) The homozygous M712T mutation of UDP-*N*-acetylglucosamine 2-epimerase/*N*-acetylmannosamine kinase results in reduced enzyme activities but not in altered overall cellular sialylation in hereditary inclusion body myopathy. *FEBS Lett.*, **566**, 105–109.
20. Schwarzkopf, M., Knobeloch, K.P., Rohde, E., Hinderlich, S., Wiechens, N., Lucka, L., Horak, I., Reutter, W. and Horstkorte, R. (2002) Sialylation is essential for early development in mice. *Proc. Natl Acad. Sci. USA*, **99**, 5267–5270.
21. Mirabella, M., Alvarez, R.B., Bilak, M., Engel, W.K. and Askanas, V. (1996) Difference in expression of phosphorylated tau epitopes between sporadic and hereditary inclusion-body myopathies. *J. Neuropathol. Exp. Neurol.*, **55**, 774–786.
22. Akanas, V. and Engel, W.K. (2006) Inclusion-body myositis: a myodegenerative conformational disorder associated with Abeta, protein misfolding, and proteasome inhibition. *Neurology*, **66** (suppl. 1), S39–S48.
23. Askanas, V. and Engel, W.K. (2003) Hereditary inclusion myopathies. In Rosenberg, R.N., Prusiner, S.B., DiMauro, S., Barchi, R.L. and Nestler, E.J. (eds), *The Molecular and Genetic Basis of Neurologic and Psychiatric Disease*, 3rd edn. Butterworth-Heinemann, Woburn, MA, pp. 501–509.
24. Akanas, V. and Engel, W.K. (2003) Proposed pathogenic cascade of inclusion-body myositis: importance of amyloid-beta, misfolded proteins, predisposing genes, and aging. *Curr. Opin. Rheumatol.*, **15**, 734–744.
25. Horstkorte, R., Nöhring, S., Wiechens, N., Schwarzkopf, M., Danker, K., Reutter, W. and Lucka, L. (1999) Tissue expression and amino acid sequence of murine UDP-*N*-acetylglucosamine-2-epimerase/*N*-acetylmannosamine kinase. *FEBS*, **260**, 923–927.
26. Ishii, A., Hagiwara, Y., Saito, Y., Yamamoto, K., Yuasa, K., Sato, Y., Arahata, K., Shoji, I., Nonaka, I. *et al.* (1999) Effective adenovirus-mediated gene expression in adult murine skeletal muscle. *Muscle Nerve*, **22**, 592–599.
27. Kimpara, T., Imamura, T., Tsuda, T., Sato, K. and Tsuburaya, K. (1993) Distal myopathy with rimmed vacuoles and sudden death — report of two siblings. *Rinsho Shinkeigaku*, **33**, 886–890.
28. Nishino, I., Malicdan, M.C., Murayama, K., Nonaka, I., Hayashi, Y.K. and Noguchi, S. (2005) Molecular pathomechanism of distal myopathy with rimmed vacuoles. *Acta Myol.*, **24**, 80–83.
29. Sugarman, M., Kitazawa, M., Baker, M., Caiozzo, V.J., Querfurth, H.W. and LaFerla, F.M. (2006) Pathogenic accumulation of APP in fast twitch muscle of IBM patients and a transgenic model. *Neurobiol. Aging*, **27**, 423–432.
30. Post, J.A. (1992) Removal of sarcolemmal sialic acid residues results in a loss of sarcolemmal functioning and integrity. *Am. J. Physiol.*, **263**, H147–H152.
31. Bennett, E., Urean, M.S., Tinkle, S.S., Kozkowski, A. and Levinson, S. (1997) Contribution of sialic acid to the voltage dependence of sodium channel gating: a possible electrostatic mechanism. *J. Gen. Physiol.*, **109**, 327–343.
32. Nishino, I. (2003) Autophagic vacuolar myopathies. *Curr. Neurol. Neurosci. Rep.*, **3**, 64–69.

33. Askanas, V., Alvarez, R.B. and Engel, W.K. (1993) β-Amyloid precursor epitopes in muscle fibers of inclusion body myositis. *Ann. Neurol.*, **34**, 551–560.
34. Askanas, V. and Engel, W.K. (1995) New advances in the understanding of sporadic inclusion-body myositis and hereditary inclusion-body myopathies. *Curr. Opin. Rheumatol.*, **7**, 486–496.
35. Ellis, R. and Pinheiro, T.J.T. (2002) Danger: misfolding proteins. *Nature*, **416**, 483–484.
36. Brooks, S.A., Dwek, M.V. and Schumacher, U. (2002) *Functional and Molecular Glycobiology*. BIOS Scientific Publishers Limited, Oxford. UK.
37. Helenius, A. and Aebi, M. (2004) Roles of N-linked glycans in the endoplasmic reticulum. *Annu. Rev. Biochem.*, **73**, 1019–1049.
38. Kumamoto, T.F.S., Nagao, S., Masuda, T., Sugihara, R., Ueyama, H. and Tsuda, T. (1998) Proteasomes in distal myopathy with rimmed vacuoles. *Intern. Med.*, **37**, 746–752.
39. Askanas, V., Engel, W.K. and Alvarez, R.B. (1993) Enhanced detection of Congo-red-positive amyloid deposits in muscle fibers of inclusion body myositis and brain of Alzheimer's disease using fluorescence technique. *Neurology*, **43**, 1265–1267.
40. Gregori, L., Hainfeld, J.F., Simon, M.N. and Goldbager, D. (1997) Binding of amyloid β protein to the 20S proteasome. *J. Biol. Chem.*, **272**, 58–62.
41. Wang, Y.P., Wang, X.C., Tian, Q., Yang, Y., Zhang, Q., Zhang, J.Y., Zhang, Y.C., Wang, Z.F., Wang, Q., Li, H. *et al.* (2006) Endogenous overproduction of β-amyloid induces tau hyperphosphorylation and decreases the solubility of tau in N2a cells. *J. Neural. Transm.*, **113**, 1723–1732.
42. McFarlane, I., Georgopoulou, N., Coughlan, C.M., Gillian, A.M. and Breen, K.C. (1999) The role of the protein glycosylation state in the control of cellular transport of the amyloid beta precursor protein. *Neuroscience*, **90**, 15–25.
43. Pahlsson, P. and Spitalnik, S.L. (1996) The role of glycosylation in synthesis and secretion of beta-amyloid precursor protein by Chinese hamster ovary cells. *Arch. Biochem. Biophys.*, **331**, 177–186.
44. Yazaki, M., Tagawa, K., Maruyama, K., Sorimachi, H., Tsuchiya, T., Ishiura, S. and Suzuki, K. (1996) Mutation of potential N-linked glycosylation sites in Alzheimer's disease amyloid precursor protein (APP). *Neurosci. Lett.*, **221**, 57–60.
45. Nakagawa, K., Kitazume, S., Oka, R., Maruyama, K., Saido, T.C., Sato, Y., Endo, T. and Hashimoto, Y. (2006) Sialylation enhances the secretion of neurotoxic amyloid-beta peptides. *J. Neurochem.*, **96**, 924–933.
46. Georgopoulou, N., McLaughlin, M., McFarlane, I. and Breen, K.C. (2001) The role of post-translational modification in beta-amyloid precursor protein processing. *Biochem. Soc. Symp.*, **67**, 23–36.
47. Tsai, B., Ye, Y. and Rapoport, T.A. (2002) Retro-translocation of proteins from the endoplasmic reticulum into the cytosol. *Nat. Rev. Mol. Cell Biol.*, **3**, 246–255.
48. Soeiro, M.N., Silva-Filho, F.C. and Meirelles, M.N. (1994) The nature of anionic sites and the endocytic pathway in heart muscle cells. *J. Submicrosc. Cytol. Pathol.*, **26**, 121–130.
49. Marengo, F.D., Wang, S.Y., Wang, B. and Langer, G.A. (1998) Dependence of cardiac cell Ca^{2+} permeability on sialic acid-containing sarcolemmal gangliosides. *J. Mol. Cell Cardiol.*, **30**, 127–137.
50. Woods, W.T., Inamura, K. and James, T.R. (1982) Electrophysiological and electron microscopic correlations concerning the effects of neuraminidase on canine heart cells. *Cir. Res.*, **50**, 228–231.
51. Ufret-Vincenty, C.A., Baro, D.J. and Santana, L.F. (2001) Differential contribution of sialic acid to the function of repolarizing K^+ currents in ventricular myocytes. *Am. J. Physiol. Cell Physiol.*, **281**, C464–C474.
52. Niwa, H., Yamamura, K. and Miyazaki, J. (1991) Efficient selection for high-expression transfectants with a novel eukaryotic vector. *Gene*, **108**, 193–199.
53. Hara, S., Yamaguchi, M., Takemori, Y., Nakamura, M. and Ohkura, Y. (1986) Highly sensitive determination of *N*-acetyl- and *N*-glycolylneuraminic acids in human serum and urine and rat serum by reversed-phase liquid chromatography with fluorescence detection. *J. Chromatogr.*, **377**, 111–119.
54. Keppler, O.T., Hinderlich, S., Langner, J., Schwartz-Albiez, R., Reutter, W. and Pawlita, M. (1999) UDP-GlcNAc 2-epimerase: a regulator of cell surface sialylation. *Science*, **284**, 1372–1376.

Congenital neuromuscular disease with uniform type 1 fiber and *RYR1* mutation

I. Sato, MD
S. Wu, MD
C.A. Ibarra M., MD, PhD
Y.K. Hayashi, MD, PhD
H. Fujita, MD
M. Tojo, MD
S.J. Oh, MD
I. Nonaka, MD, PhD
S. Noguchi, PhD
I. Nishino, MD, PhD

Address correspondence and reprint requests to Dr. I. Nishino, Department of Neuromuscular Research, National Institute of Neuroscience, National Center of Neurology and Psychiatry (NCNP), 4-1-1 Ogawahigashi-cho, Kodaira, Tokyo 187-8502, Japan
nishino@ncnp.go.jp

ABSTRACT

Background: Congenital neuromuscular disease with uniform type 1 fiber (CNMDU1) is a rare form of congenital myopathy, which is pathologically diagnosed by the presence of more than 99% of type 1 fiber, with no specific structural changes. Its pathogenic mechanism is still unknown. We recently reported that almost all patients with central core disease (CCD) with ryanodine receptor 1 gene (*RYR1*) mutations in the C-terminal domain had type 1 fibers, nearly exclusively, in addition to typical central cores.

Objective: To investigate whether CNMDU1 is associated with *RYR1* mutation.

Methods: We studied 10 unrelated Japanese patients who were diagnosed to have CNMDU1 based on clinical features and muscle pathology showing more than 99% type 1 muscle fibers. We extracted genomic DNA from frozen muscles and directly sequenced all 106 exons and their flanking intron-exon boundaries of *RYR1*.

Results: Four of 10 patients had a heterozygous mutation, three missense and one deletion, all in the C-terminal domain of *RYR1*. Two missense mutations were previously reported in CCD patients. Clinically, patients with mutations in *RYR1* showed milder phenotype compared with those without mutations.

Conclusion: Congenital neuromuscular disease with uniform type 1 fiber (CNMDU1) in 40% of patients is associated with mutations in the C-terminal domain of *RYR1*, suggesting that CNMDU1 is allelic to central core disease at least in some patients.

***Neurology*® 2008;70:114-122**

Congenital neuromuscular disease with uniform type 1 fiber (CNMDU1) was first described in 1983.[1] It is a rare disorder pathologically characterized by the exclusive presence of type 1 muscle fiber (>99%) without any specific structural abnormality such as cores, nemaline bodies, or centrally placed nuclei. Clinically, it shares common features with congenital myopathy; including early onset, mild proximal muscle weakness, hypo- or areflexia, normal creatine kinase levels, and myopathic electromyography findings. So far, at least 12 cases have been reported.[1-10] However, its genetic cause and molecular pathomechanism are still unknown.

We are aware of a rare existence of CNMDU1 case with a family history of central core disease (CCD) in our own series[6] and in the previous report.[7] In addition, our recent study on CCD revealed that patients with a heterozygous C-terminal mutation in the gene encoding ryanodine receptor 1 (*RYR1*) have nearly exclusively type 1 fibers, in addition to well-demarcated, mostly singular and centrally located, "typical" cores,[11]

Editorial, see page 99

e-Pub ahead of print on May 30, 2007, at www.neurology.org.

From the Department of Neuromuscular Research (I.S., S.W., C.A.I.M., Y.K.H., I.N., S.N., I.N.), National Institute of Neuroscience, National Center of Neurology and Psychiatry, Kodaira, Department of Pediatrics (I.S.), Tohoku University School of Medicine, Sendai, Department of Pediatrics (H.F.), Hirosaki University School of Medicine, Department of Pediatrics (M.T.), Niigata Prefecture Hamagumi Medical Rehabilitation Center for Handicapped Children, Japan; and Department of Neurology (S.J.O.), University of Alabama at Birmingham.

Supported by "Research on Psychiatric and Neurological Diseases and Mental Health" from Health and Labor Sciences Research Grants; "Research on Health Sciences Focusing on Drug Innovation" from the Japanese Health Sciences Foundation; "Research Grant (16B-2, 17A-10) for Nervous and Mental Disorders" from the Ministry of Health, Labor, and Welfare; and the Program for Promotion of Fundamental Studies in Health Sciences of the National Institute of Biomedical Innovation (NIBIO).

Disclosure: The authors report no conflicts of interest.

suggesting a tight relationship between uniform type 1 fiber and *RYR1* mutations, especially those in the C-terminal domain. We therefore hypothesized that CNMDU1 may be caused by *RYR1* mutation.

METHODS Subjects. All clinical materials used in this study were obtained for diagnostic purpose with informed consent. Ten unrelated Japanese patients (seven boys and three girls) were diagnosed to have CNMDU1 among 9,300 frozen muscle biopsies diagnosed at National Center of Neurology and Psychiatry (NCNP) from 1976 to 2005. The diagnosis was established based on clinical and pathologic findings of muscle specimens consistent with CNMDU1 described previously.[1] Clinical features of the patients were assessed by the information provided by the physicians. Pathologic features of all patients were independently evaluated by three authors. A battery of histochemical stains was performed on biopsied muscle specimens from all patients, including hematoxylin and eosin, modified Gomori trichorome, nicotinamide adenine dinucleotide-tetrazolium reductase, and myosin ATPase. We counted the total number of muscle fibers and that of each fiber type in one section to accurately calculate the percentage of type 1 fibers. Muscle sample for electron microscopic analysis was available only in Patient 3.

Patients underwent muscle biopsy because of hypotonia since birth (4/10) or delayed motor milestones (6/10). Age at biopsy varied from 5 months to 13 years with a mean age of 3.3 ± 3.8 years old (mean ± SD, n = 10).

Patients 2 and 4 had family history of neuromuscular disease. The father of Patient 2 had muscle weakness of unknown origin. Regarding Patient 4, the father was previously diagnosed to have CCD and the brother had similar clinical manifestations to the patient, although muscle sample was not available. None of the patients had past or family history of malignant hyperthermia (MH) or MH susceptibility. Nine had perinatal history: poor fetal movement (5/9), asphyxia (4/10), hypotonia (7/9), and weak suck (8/9). Six had respiratory distress; five of them experienced acute respiratory distress requiring mechanical ventilation; three (Patients 5, 7, and 8) had asphyxia at birth, two (Patients 6 and 10) developed infection during childhood, and one (Patient 1) had wheezing during neonatal period. All had muscle weakness and delayed motor milestones. Skeletal deformity (9/10), myopathic facies (7/9), and high arched palate (7/9) were also frequently observed. Patient 9 had exotropia. Five had mental retardation. Brain imaging was performed in these five patients, and we have seen dilatation of the ventricles (Patients 7 and 8) and brain atrophy (Patient 9). Patients 5 and 6 had no abnormality. Patient 8 had an episode of interventricular hemorrhage in the perinatal period. Moreover, no patient had epileptic episode, and Patient 9 showed normal EEG findings. All patients showed hypo- or areflexia. Serum creatine kinase level was within normal range in all. Only one patient (Patient 5) underwent muscle biopsy twice initially at 5 months and later at 2 years 9 months, both providing the same diagnosis (CNMDU1). The detailed clinical information of Patients 4,[7] 6,[8] and 9[9] was previously described elsewhere.

Mutation analysis. Genomic DNA was extracted from muscle biopsy samples according to standard protocols.[1] All 106 exons of *RYR1* and their flanking regions (GenBank GeneID 6261) were amplified and directly sequenced as described previously.[7,10] We also analyzed DNA from two patients with congenital myopathy with marked type 1 fiber predominance (96% and 97%) but without any other specific pathologic abnormalities such as type 1 fiber atrophy, nemaline body, centrally placed nuclei, and cores. DNA samples from 150 subjects apparently without any neuromuscular disorders and those from 2 patients with congenital myopathy with marked type 1 fiber predominance were used as controls. We also performed mutation screening in exons 1 to 4 of *FKBP1A* (GenBank Gene ID 2280), encoding FK506-binding protein 1A (12 kd), and exons 14 to 17 and 25 to 27 of *CACNA1S* (GenBank Gene ID 779), encoding the α_1S subunit of L-type voltage-dependent calcium channel or dihydropyridine receptor, both of which span the *RYR1*-interacting region. DNA from family members was available only in Patient 1. In addition, we extracted genomic DNA from paraffin-embedded muscles of the original three patients[1] and attempted to directly sequence the C terminal domain, exons 90 to 106 of *RYR1*.[10]

Total RNA was extracted from biopsied muscle using standard technique and reversely transcribed into cDNA using SuperScript III First-Strand Synthesis System for reverse transcription PCR (Invitrogen, Carlsbad, CA). Four overlapping fragments spanning exons 89 to 106 (nucleotides 12,220 to 12,819, 12,719 to 13,419, 13,351 to 14,350, 14,251 to 15,170) were amplified from the first-strand cDNAs.

PCR-amplified fragments were directly sequenced using BigDye Terminator v3.1 Cycle Sequencing kits on ABI3100 automated Genetic Analyzer (Applied Biosystems, Foster City, CA). Sequences were analyzed with the SeqScape program in comparison with the reference sequences of *RYR1*, *FKBP1A*, and *CACNA1S*.

To rule out the presence of polymorphisms, we sequenced all the exons carrying novel sequence variations in 150 control DNAs without any known neuromuscular disorder. We also used the Japanese Single Nucleotide Polymorphisms database for checking common gene variations in the Japanese population.[15]

To confirm the mutations of Patients 1 and 4, the PCR products of mutant *RYR1* were cloned into plasmid pGEM-T (Promega, Madison, WI) and direct sequencing of the cloned fragments was performed.

Western blot analysis of RYR1 protein. Solubilized proteins (approximately 50 μg) from five slices (6 μm thick) of frozen muscles (Patients 1 and 3) were loaded onto 5% sodium dodecyl sulfate polyacrylamide gels, electrophoresed, transferred onto polyvinylidene fluoride membranes, and hybridized with primary mouse monoclonal anti-RYR antibody (34C; Developmental Studies Hybridoma Bank, University of Iowa, Iowa City, IA; 1:100).[16] A horseradish peroxidase goat anti-mouse IgG (Zymed Laboratories, San Francisco, CA) was used as secondary antibody. The immunoreactive bands on the membrane were visualized using Las-1000 Pro (Fujifilm, Tokyo) by enhanced chemiluminescence (Amersham Bioscience Buckinghamshire, UK) as recommended by manufacturer. The intensity of the RYR bands was quantified by densitometric analysis using Quantity One (PDI, Huntington, NY). One muscle sample without any neuromuscular disorder was used as control.